Photoionization of atomic barium: Ba atoms in the ground state

J. M. Bizau, D. Cubaynes, P. Gérard, and F. J. Wuilleumier
Laboratoire de Spectroscopie Atomique et Ionique, Université Paris–Sud, Bâtiment 350, 91405 Orsay CEDEX, France
and Laboratoire pour l'Utilisation du Rayonnement Electromagnétique, Université Paris–Sud, Bâtiment 209d, 91405 Orsay CEDEX, France
(Received 2 March 1989)

We present detailed experimental results for the photoionization processes of barium atoms in the ground state, from 16 to 180 eV photon energy. Using electron spectroscopy, we have measured partial photoionization cross sections for the 6*s*, 5*p*, 5*s*, and 4*d* subshells, including satellite to main-line branching ratios and 5*p* and 4*d* Auger spectra. These results reveal, in particular, significantly lower values of the 4*d* photoionization cross section than previously predicted by a number of theoretical calculations, or deduced from photoabsorption data. They are, however, in better agreement with two most recent, yet unpublished, calculations. A particular care has been brought to the regions of 5*p* and 4*d* discrete electron excitations, where the excitation functions of the main Ba^+ exit channels, and also of the Ba^{2+} decay channel in the case of 5*p* excitations, have been studied. Finally, we have measured the oscillator strength for excitation of some isolated 5*p* resonances and for the whole 5*p* subshell.

I. INTRODUCTION

In the paper presented here, we give the first part of an extensive x-ray photoelectron spectrometry (XPS) study of photoionization processes in barium atoms, both in the ground state and in excited states, using synchrotron radiation between 16 and 180 eV photon energy. The results on the excited barium have been obtained with the now well-established method combining the use of laser and synchrotron radiations.[1–3] They are planned to be presented in a following paper.[4] Here, we present the data measured for barium atoms in the ground state.

Neglecting initial-state configuration interaction (ISCI), the Ba ground-state configuration may be written as

$$|\Phi\rangle = 1s^2 \cdots 4d^{10}5s^2 5p^6 6s^2\,{}^1S_0 \ . \tag{1}$$

All alkaline-earth atoms, like barium, have two electrons in the filled outer *s* subshell outside a rare-gas-like inner core. This makes the interpretation of photoionization processes easier for these atomic systems than for open-subshell atomic metals. Nevertheless, they are open-shell atoms. In the particular case of barium, the 6*p*, 5*d* and 4*f* levels are empty and play an important role for most of the strong many-electron effects observed.[5]

(i) Large polarizability of the 6*s*, 5*p*, and 4*d* subshells due to their close localization in the same region of space with the 6*p*, 5*d*, and 4*f* empty levels, respectively.[6] In first approximation, this would result in the existence of $6s \rightarrow 6p$, $5p \rightarrow 5d$, and $4d \rightarrow 4f$ "giant" resonances. For the first two types of transition, the resonance effects appear in the discrete part of the excitation spectrum. For the transitions from the 4*d* subshell, the increase of angular momentum in the final state shifts the oscillator strength into the continuum part of the spectrum. Another effect of the polarization is to screen the external field, then strongly affecting the 6*s*-5*p*-5*s* and 4*d* photoionization cross sections.

(ii) Collapse of the 5*d* subshell upon core excitation or ionization, leading to strong interaction between the $6s^2$, $6s5d$, and $5d^2$ configurations. This effect is responsible for the spread of the oscillator strength of the $5p \rightarrow 5d$ giant dipole resonance over a wide number of $5p^5 n_1 l_1 n_2 l_2 n_3 l_3$ excited atomic states of Ba*.[7,8] Another interesting aspect is that the electron transfer of the $6s \rightarrow 5d$ or $6s^2 \rightarrow 5d^2$ type may lead to lowering of the total energy of some $Ba^+(nl^{-1})$ ionic states, where nl^{-1} stands for the core hole. One therefore finds that there is a number of *nl* ionization limits at energies lower (due to this so-called shake-down effect) as well as at energies higher (shake-up states) than the most probable *nl* ionization limit due to the removal of a single electron.

Thus it is not surprising if a huge number of theoretical and experimental studies on photoionization of Ba have been dealing with 6*s*, 5*p*, or 4*d* discrete or near-threshold electron excitation. The intermediate photon energy regions concerned with direct ionization have been less studied. In the same way, and from the experimental aspect, most of the results have been obtained using photoabsorption spectroscopy.[7–11] It should be noted, however, that none of these measurements has provided truly absolute cross sections. Only the relative variation of the total photoabsorption cross section, i.e., its photon energy dependence, has been measured. The absolute values, which have been published, have always been obtained by way of normalization to some theoretical result or to some sum rule, and it is still the case for all recent works on barium.

Theoretical results have been very scarce in the 5*p* excitation region,[12,13] and numerous in the 4*d* threshold region, using many different approximations.[5,6,13–21] The

calculations including relaxation effects better reproduce the total photoabsorption measurements.[15,18–20] However, the crucial test of the theory must be done in comparing calculated and measured partial photoionization cross sections,[22,23] i.e., the cross sections for ejection of a given nl electron with the positive ion being left in a given final state. This goal can be reached only when a differential analysis, such as the one provided by electron spectrometry, is used to determine the branching ratios of all possible processes and to partition the total cross section into its various components: photoelectron spectrometry is the only method which allows a complete identification of nonradiative exit channels in resonant or in direct single ionization. For barium, few data are available from photoelectron spectroscopy, mostly at discrete photon energies using rare-gas emission lines,[24–27] and in narrow bands of photon energies using synchrotron radiation in the $5p$ excitation region[28,29] or above the $4d$ thresholds,[30,31] with one experiment on solid barium.[32]

The great tunability of synchrotron radiation authorizes the study of photoionization processes over an extended energy range, as well as the excitation of well-defined autoionizing resonances at selected energies. The efficiency of these two tools was widely demonstrated by a recent photoemission study of atomic calcium.[33,34] We will refer frequently to this work on a lighter alkaline-earth atom to interpret our results on barium atoms, all the more because numerous similar many-electron effects of the types quoted above have been studied in the case of calcium (collapse of the $3d$ empty subshell, shake-down process, $3p \rightarrow 3d\ ^1P$ giant resonance).

The various processes involved in the photoionization of barium atoms in the ground state may be summarized, following the simplified photoexcitation and decay schemes:

$$\begin{array}{ccc} \mathrm{Ba} + h\nu & \xrightarrow{a} & \mathrm{Ba^+(nl^{-1}) + e^-\ (\varepsilon)} \\ \downarrow c \quad \searrow f & \nearrow d \quad \searrow b & \\ \mathrm{Ba^*\ (n_1l_1^{-1}\ n_2l_2)} & \xrightarrow[e]{} & \mathrm{Ba^{m+} + pe^-\ (\varepsilon)} \end{array} \qquad (2)$$

where the different paths have the following meaning.

(a) Direct single ionization in the nl subshell.

(b) Direct multiple ionization.

(c) Resonant excitation of a n_1l_1 electron to a n_2l_2 empty orbital (transition $n_1l_1 \rightarrow n_2l_2$) leaving the Ba atom in an excited state.

(d) and (e) Decay channels of the $n_1l_1^{-1}n_2l_2$ Ba* resonance via single and multiple ionization.

(f) Auger decay of the hole created by inner-shell ionization.

In this scheme, radiative decays are not indicated. They compete with nonradiative decays (d), (e), and (f), and they have not been studied in this work.

Many of these processes are illustrated in the electron spectrum we have obtained at $h\nu = 130.2$ eV, shown in Fig. 1. This photon energy is far greater than the binding energy of $nl = 6s$, $5p$ $5s$, and $4d$ electrons in barium atom, and does not coincide with any resonant excitation. Thus we observe electron lines arising from direct single ionization in these different subshells [process (a)] with respective kinetic energy of 125 eV (line labeled $6s^{-1}$), 107 eV ($5p^{-1}$), 92 eV ($5s^{-1}$), and 30 eV ($4d^{-1}$). The $5p^{-1}$ and $4d^{-1}$ lines are split by spin-orbit interaction into two components $5p_{1/2}$, $5p_{3/2}$ and $4d_{3/2}$,$4d_{5/2}$. During direct ionization, one (or even two) outer electrons may be promoted to an empty level, giving rise to the so-called "satellite" photoelectron lines. An example is

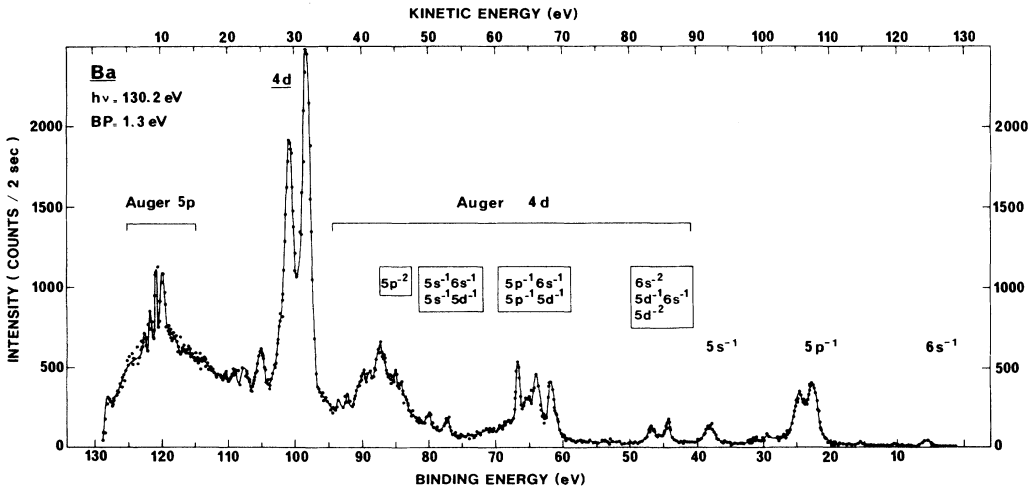

FIG. 1. Electron spectrum recorded at 130.2 eV photon energy. The observed lines arise from direct photoionization in the $4d$, $5s$, $5p$, and $6s$ subshells, and from Auger decay of the $5p$ and $4d$ holes. As in the other figures, BP is the spectral bandpass of the monochromator.

given by the lines between 19 and 25 eV kinetic energy, corresponding to $4d$ ionization plus excitation of one or two $6s$ electrons ($4d$ satellites corresponding to $4d^9 5s^2 5p^6 nln'l'$ final Ba^+ ionic states). Finally, lines from 5 to 15 eV and from 40 to 90 eV kinetic energy arise from Auger decay of $5p$ and $4d$ holes, respectively [process (f)].

After a short description of the experimental apparatus and of the data treatment, we divide the presentation of the results into two parts. First, we discuss the direct ionization in the $6s$, $5p$, $5s$, and $4d$ subshells. This section includes also the study of the Auger decay of the core holes. The second part is devoted to resonant ionization following $5p$ and $4d$ electron excitations.

II. EXPERIMENTAL PROCEDURE

A. Experimental setup

The experimental apparatus and the data treatment we used have been widely described in Ref. 34. Briefly, ionizing photons were provided by the Anneau de Collision d'Orsay (ACO) storage ring at the synchrotron radiation facility Laboratoire pour l'Utilisation du Rayonnement Electromagnétique (LURE). Synchrotron radiation was monochromatized by a 1-m grazing-incidence toroidal grating monochromator. The bandpass was varied between 1% of the photon energy and 0.35% in the region of $5p$ electron excitation. The photon flux was contineously monitored at the exit of the monochromator, using an 80% transmission gold mesh, whose photoelectric yield is known. The Ba atoms were produced in a stainless-steel furnace, heated at about 830 K. It gave an effusive beam of some 10^{12} atoms/cm^3, collinear to the monochromatized synchrotron radiation beam. The electrons emitted around the "magic angle" of 54° 44′ in the interaction of these two beams were energy analyzed by a cylindrical mirror analyzer (CMA). This geometry makes the measured intensity of the electron signals independent of the polarization of the synchrotron light and of the angular distribution of the photoelectrons. The resolution of the electron spectrometer was kept constant, at 1% of the kinetic energy of the analyzed electrons.

B. Data treatment

Electron spectra similar to the one shown in Fig. 1 have been taken at regular energy intervals over the whole photon energy range studied in this work, the energy step being much smaller in the resonant parts than in the continuum parts of the excitation processes. The main information obtained from the analysis of the spectra is the binding energies of the atomic states and the branching ratios for photoionization or nonradiative decay into the different ionic channels.

In order to extract relative photoionization cross sections from the detected electron signal, we have to know (i) the proportion of higher-order photons diffracted by the monochromator at each photon energy, only the sum of them being measured by the gold mesh; (ii) the relative transmission of the spectrometer versus the electron kinetic energy. These two points were systematically studied, using the photoelectron signal produced in rare gases of known photoionization cross section. In addition, we checked any possible variation of the vapor density in the interaction volume by recording, at regular intervals, a barium photoelectron spectrum always at the same photon energy. The photoelectron signal from the rare gases was also used to determine the absolute kinetic energy scale of the spectrometer, as well as an accurate value of the photon energy. This was necessary because of the deposition of Ba vapor on the entrance slits of the spectrometer, which results in a contact potential decelerating the electrons. The partial cross sections for photoionization of barium into the different continuum channels were obtained, on a relative scale, from the integrated area under the corresponding photoelectron lines, after proper experimental corrections and normalizations.

Absolute values of the partial cross sections cannot be determined accurately with electron spectrometry alone. But there is no accurate measurement of the absolute photoabsorption cross section of atomic Ba in the photon energy range we consider here. Thus, in order to obtain absolute partial photoionization cross sections, we have to normalize one of the relative photoionization cross sections to the results of some theoretical calculations. We chose the $5p$ subshell photoionization cross section, because there is an overall agreement on this cross section among most of the existing theoretical calculations and because we have measured it over an extended energy scale. We normalized our experimental data to the values calculated using the local-density random-phase approximation[5] (LDRPA). Figure 2 illustrates this procedure. Our measurements are placed on an absolute scale in determining the multiplication factor giving the best fit to the theoretical curve on the whole 50–140-eV energy range. The experimental points are obtained as the sum of the intensity of main lines plus satellite lines in the $5p$ photoelectron spectra. We will see in Sec. IV A that this procedure is consistent with a total oscillator strength (continuum + discrete transitions) of 6 for the $5p$ subshell. The absolute photoionization cross sections in

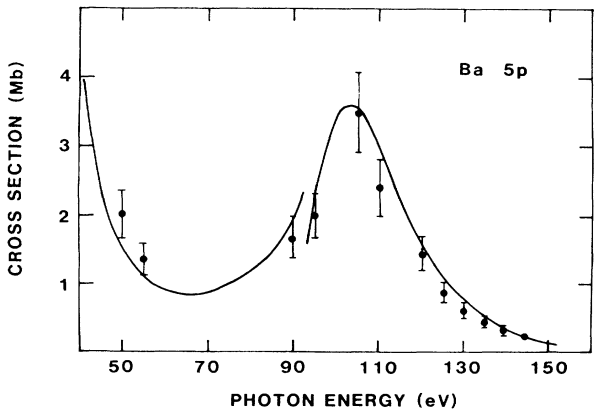

FIG. 2. Experimental and theoretical data for the $5p$ cross section used for the normalization procedure of all cross sections measured in this work (theory is from Ref. 5).

the other subshells are then obtained from the branching ratios $Ba^+(nl^{-1})$:$Ba^+(5p^{-1})$ we measured in our spectra.

III. DIRECT PHOTOIONIZATION: RESULTS AND DISCUSSION

A. Photoionization in 6s subshell

Photoionization processes in the 6s subshell of atomic barium may be represented by

$$5p^6 6s^2\,{}^1S_0\ \mathrm{Ba} + h\nu \rightarrow 5p^6 nl\,{}^2L_J\ \mathrm{Ba}^+ + e^- , \qquad (3)$$

where $nl = 6s$ stands for single ionization; ionization accompanied by excitation to the nl empty orbitals gives rise to the satellite electron lines. Because of the low intensity of this last process, we have not been able to observe any line corresponding to satellite states more excited than the $nl = 5d$ one at high photon energy, in the continuum. Their intensity has been measured, nevertheless, in great details in the region of resonant excitation of a 5p electron where they are strongly enhanced [processes (2c) and (2d)]. The binding energies of the $5p^6 nl$ states are accurately known from optical data.[35] They are listed in Table I.

1. Photoionization cross sections

The variation with photon energy of the 6s photoionization cross section is shown in Fig. 3. Our experimental measurements are obtained as the sum of the main-line ($nl = 6s$) plus 5d satellite-line intensities. They are compared with a one-electron calculation,[36] using relativistic Herman-Skillman potential and with a many-electron calculation developed in the LDRPA.[5] The results of another one-electron calculation,[37] not shown in the figure, are close to the first one. Even though, in the nonresonant part of the ionization region, around 40 eV, the one-electron calculations appear to be in better agreement with the experimental results, the LDRPA calculation is the only one able to correctly reproduce the general behavior of the cross section, because of the strong effects of the interchannel coupling.

TABLE I. Binding energies and assignments of the first $5p^6 nl\,{}^2L_J$ Ba^+ ionic states (from Ref. 35).

nl_j	Binding energy (eV)
$6s_{1/2}$	5.21
$5d_{3/2}$	5.81
$5d_{5/2}$	5.91
$6p_{1/2}$	7.72
$6p_{3/2}$	7.93
$7s_{1/2}$	10.46
$6d_{3/2}$	10.91
$6d_{5/2}$	10.93
$4f_{5/2}$	11.19
$4f_{7/2}$	11.22
$7p_{1/2}$	11.33
$7p_{3/2}$	11.41
$5f_{5/2}$	12.33
$5f_{7/2}$	12.36
$8s_{1/2}$	12.40
$7d_{5/2}$	12.62
$7d_{7/2}$	12.64
$5p^6\,{}^1S_0$ Ba^{2+}	15.215

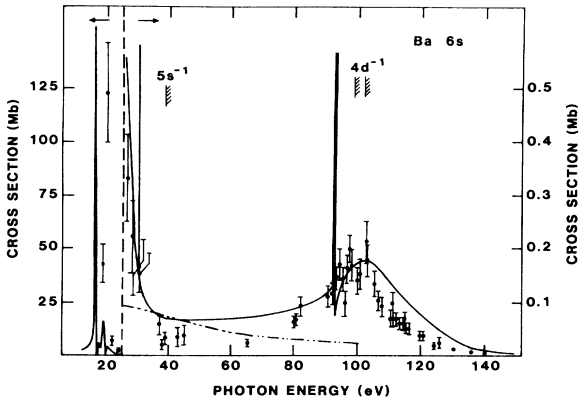

FIG. 3. Variation of the 6s photoionization cross section of atomic barium. ⧓, present work. Theoretical curves are the result of one-electron calculation, Ref. 36 (— ·· —) and LDRPA calculation, Ref. 5 (——).

- Below 40 eV, the fast decrease of the cross section accounts for the wing of the giant resonance $5p \rightarrow 5d$. This region, dominanted by 5p excitations, is discussed in detail in Sec. IV A; only a few measurements are shown here.
- Above 100 eV, the enhancement of the cross section results from the opening of the $4d \rightarrow \epsilon l$ channels (the position of the main ionization thresholds we have measured are indicated by vertical bars at the top of the figure).

From the combination of these two effects, there results a minimum around 40 eV, which is itself perturbated by interchannel coupling with the Cooper minimum in the $5p \rightarrow \epsilon l$ channels, and by the opening of the $5s \rightarrow \epsilon p$ channel. The true Cooper minimum in the 6s cross section is expected to be at much lower photon energy.[38]

The LDRPA calculation, which introduces most of these interchannel effects, reproduces qualitatively well the behavior of the cross section. Nevertheless, in the flatter 50–80-eV and 120–140-eV regions, where no important resonant excitation perturbs the direct photoionization process, the LDRPA result is often a factor of 2 higher than our measurements. This may be due to a tendency of the LDRPA approximation to overestimate the interchannel coupling, as we have noted earlier in the cases of 4s and 3s photoionization cross sections in Ca.[34] The large intensity of the resonances $5s \rightarrow 6p$ at 30.9 eV in the calculation would be greatly reduced if the Auger width of the 5s hole would be taken into account. This is also true for the $4d \rightarrow 6p$ resonances near 92 eV.

2. Branching ratios

The variation of the branching ratio between the 5d satellite line ($5p^6 5d\,{}^2D_{3/2,5/2}$ Ba^+ ionic states) and the

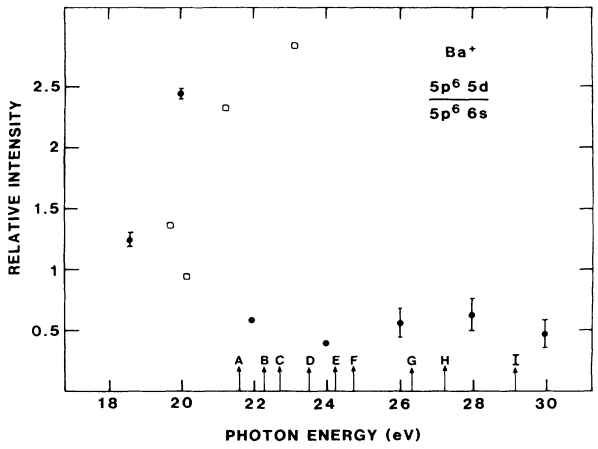

FIG. 4. Variation of the $(5p^6 5d : 5p^6 6s)$ Ba^+ branching ratio. ⧫, present work; □, from Ref. 26. The positions of the various $5p$ thresholds are indicated by the arrows at the bottom of the figure.

main line ($5p^6 6s\ ^2S_{1/2}$ Ba^+ ionic state) is reproduced in Fig. 4, between 18 and 30 eV photon energy. Below 22 eV, only two of our measurements are reported for illustration (see Sec. IV A). Some values obtained with He and Ne gas emission lines[26] are also indicated. They are not easily comparable with ours, because they are obtianed by detection of electrons emitted at 90° instead of the magic angle, and because of the presence of numerous autoionizing lines. Above 22 eV, our values are roughly constant, staying around 50%. In the final state of process (3), the Ba^+ ion is constituted of a closed core plus a single outer electron. Then final-state configuration interaction (FISCI) is likely a negligible mechanism for production of the satellite lines, compared to initial-state configuration interaction. The ISCI development of the initial state [ground state (g.s.)] of Ba has been calculated to be[39]

$$|\text{Ba g.s. } {}^1S_0\rangle = 0.94|6s^2\,{}^1S_0\rangle - 0.11|5d^2\,{}^1S_0\rangle + 0.20|6s7s\,{}^1S_0\rangle + 0.25|6p^2\,{}^1S_0\rangle + \cdots . \quad (4)$$

The constant behavior of the $5d:6s$ branching ratio with the photon energy is consistent with an ISCI origin of the $5d$ satellite. Nevertheless, its intensity is much too high compared to the 1% or 2% expected from (4). We have already met this problem earlier, in the case of the $3p^6 3d$ satellite in Ca,[33] and it has been shown that the difference between the measured intensity of the *nd* satellites in the alkaline-earth atoms and the calculated one is growing with increasing atomic numbers.[26] Such a high intensity of the $5d$ datellite might be explained by some contribution of configuration interaction between the ion and the outgoing electron (CSCI), which is difficult to quantify. But most of the difference is more likely due to the existence, in all this 24–30-eV energy region, of a high density of autoionizing resonances involving two-electron excitations, converging to the various $5p^{-1}$ ionization thresholds. The positions we have measured for these thresholds are indicated at the bottom of the figure by vertical arrows. We will go back to this question in Sec. IV A.

B. Photoionization in 5p subshell

The processes related to direct photoionization in the $5p$ subshell of barium atoms can be summarized into

$$5p^6\,6s^2\,{}^1S_0\ \text{Ba} + h\nu \xrightarrow{a} 5p^5\,6s^2\,{}^2P_{1/2,3/2}\ \text{Ba}^+ + e^-$$
$$\xrightarrow{b} 5p^5\ nl\ n'l'\ \text{Ba}^+ + e^- \xrightarrow{c} 5p^6\,{}^1S_0\ \text{Ba}^{2+} + e^- \quad (5)$$

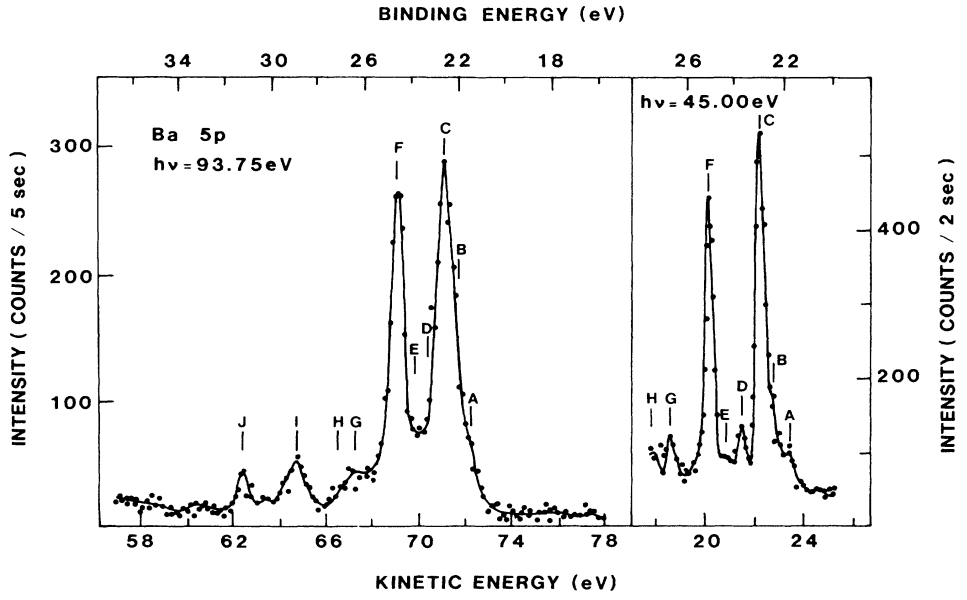

FIG. 5. Two photoelectron spectra resulting from ionization in the $5p$ subshell, recorded at 93.75 and 45 eV photon energies.

1. Photoelectron spectra

Two $5p$ photoelectron spectra, recorded with different resolution, are shown in Fig. 5. They correspond to the 20–35-eV binding energy region in the full spectrum of Fig. 1.

Process (5a) corresponds to the $5p_{3/2}$ and $5_{1/2}$ main lines, labeled C and F in the spectra. Process (5b) gives rise to the satellite lines, at higher binding energy (lines $G-J$) as well as at lower binding energy (e.g., lines A and B). These last ones, the so-called "shake-down satellites," result from the collapse of the $5d$ orbital below the $6s$ orbital in the presence of a $5p$ hole. The binding energies we have measured for the various final ionic states of Ba^+ are reported in Table II (second column). They are compared with previous measurements carried out by electron impact[40] (fourth column) and by photoabsorption of Ba^+ (Ref. 41) (third column). These ionic states correspond also to the limits of autoionizing series observed in the photoabsorption spectrum of the Ba atom.[7] The assignments proposed by the authors in Ref. 7 for these limits are listed in column 5. The assignment in columns 6–9 is based on a relativistic Hartree-Fock multiconfigurational calculation[42] (MCDF). The coefficients a, b, and c are obtained from the development of the final ionic state (FISCI).

$$|5p^5nln'l',J\ Ba^+\rangle = a|5p^56s^2,J\rangle + b|5p^55d6s,J\rangle + c|5p^55d^2,J\rangle\ . \quad (6)$$

2. Auger Spectrum

The Auger decay of the $5p$ hole is described by process (5c). The resulting Auger spectrum is spread over the 6–16-eV kinetic energy region in Fig. 1. The kinetic energy of the lines we have observed are given in Table III (column 2), taking line 20 as an absolute reference.[44] The agreement with previous measurements obtained by electron impact[43,44] (columns 3 and 4) is quite satisfactory. We note that there is only one final state of spherical symmetry for the Auger decay (the next $5p^45d\ Ba^{2+}$ ionic state is at 31.9 eV).[45] Thus there is a single connection (a mirror image) between the $5p$ photoelectron spectrum and the Auger spectrum, with a better resolution however for the last one, because it is not broadened by the bandpass of the monochromator. This correspondence is outlined in column 1 of Table III where are indicated the letters of the lines given in Table I and in Fig. 5. In the same way, the series limits observed in the photoabsorption spectrum of Ba (Ref. 7) are indicated in column 5. This correspondence allows us to deduce a measurement of the $5p$ photoionization cross section from the intensity of the Auger lines, after proper correction for contributions due to higher-order photons. This is of particular interest just above the thresholds, where the photoelectron have too low a kinetic energy to be accurately analyzed by the CMA. To be correct, this assumes that the radiative decay of the $5p$ hole is negligible. We have checked this assumption to be valid, since we found that the total intensity of the $5p$ Auger spectrum is equal, within our experimental uncertainty, to the total intensity of the $5p$ photoelectron spectrum, between 30 and 100 eV photon energy.

3. Cross sections

As it is emphasized by Table II, the distinction is less obvious between main lines and satellite lines. This results from the collapse of the $5d$ orbital in the presence of the $5p$ hole, leading to a strong mixing of the $5p^56s^2$, $5p^56s5d$, and $5p^55d^2$ ionic configurations of Ba^+. However, we choose to still call main lines the lines C and F, because they correspond to the configuration having the strongest $^2P_{1/2,3/2}$ character, and because they have the highest intensity, as expected. It has not been possible, generally, to deconvolute the weak and neighboring lines

TABLE II. Binding energies and possible assignments of the $5p^5nln'l'Ba^+$ ionic states.

Lines	Binding energy[a] (eV) This work	Ref. 41	Ref. 40	Ref. 7[b]	Assignment (Ref. 42[c]) a^2	b^2	c^2	J
A	21.60(4)	21.64(1)		h	6.5	37.3	56.3	3/2
B	22.27(3)	22.229(1)		f	2.0	25.2	72.8	3/2
C	22.72(2)	22.268(1)	22.75(5)	e	24.3	30.5	45.2	3/2
		22.794(1)		d	41.0	26.3	32.6	3/2
D	23.51(3)	23.516(1)		c	9.7	51.0	39.3	1/2
E	24.20(3)	24.123(1)			3.5	63.7	32.8	3/2
F	24.75(2)	24.755(1)	24.76(2)	a,b	79.2	1.1	19.7	1/2
G	26.3(2)	26.393(1)			3.7	54.1	42.2	3/2
H	27.2(2)	27.150(2)			13.7	6.2	80.1	1/2
I	29.2(1)	29.158(3)		$5p^56p^2$ $J=3/2$	0	2.5	97.5	3/2
J	31.3(1)	31.336(3)		$5p^56p^2$ $J=1/2$				

[a]The number in parentheses gives the uncertainty on the last figure.
[b]The letters refer to the name given by the authors to the series limits.
[c]The ionic states are developed according to $a|5p^56s^2,J\rangle + b|5p^56s5d,J\rangle + c|5p^55d^2,J\rangle$.

A, B, D, and E from the main lines C and F. Thus we show in Fig. 6 the variation of the cross section for production of all lines $A-F$. The points below 30 eV photon energy are obtained from the total intensity of the Auger lines 1–22. The qualitative behavior of this cross section is characterized by a maximum at threshold, followed by a Cooper minimum around 60 eV, and, like for the $6s$ cross section, an enhancement at the opening of the $4d \rightarrow \epsilon f$ channels.

The variation, with photon energy, of the ratio between the intensity of lines C and F is presented in Fig. 7. The strong oscillating behavior of our measurements is associated with the opening of new channels (for example, the channels $5s \rightarrow \epsilon p$ around 40 eV and $4d \rightarrow \epsilon f$ around 100 eV). Here, we note particularly the oscillations between 110 and 120 eV, likely produced by double resonant excitations leading to excited atomic states of the $4d^9 5p^5 6s^2 5d^2$ Ba* type,[11,12] autoionizing to the $5p \rightarrow \epsilon l$ channels. The presence of these resonances was already observable in the $6s \rightarrow \epsilon p$ channel (see Fig. 3). Our experimental values are compared, in Fig. 7, with the results of the one-electron calculation[37] and of the LDRPA calculation.[5] Both fail to reproduce even qualitatively the behavior of this ratio. This discrepancy emphasizes the difficulty to correctly describe a heavy atom like barium: one has to take into consideration interchannel coupling between a large number of ionization channels, clearly spreading over the whole 20–140-eV energy range. Relativistic effects and configuration interaction pull the ratio far below the statistical value of 2.

Satellite lines exhibit the same general behavior as the main lines. This is attested to by the branching ratios between the intensity of the most intense satellite lines ($G+H$), I, and J relative to the intensity of the main lines, as shown in Fig. 8. Apart from the region of $4d$ electron excitation, the ratios have a rather constant value, between 6% and 8%. This would be consistent with a dominant ISCI origin suggested for the G and H satellites (see Table II). For the assignment of the I and J satellites, the $5p^5 6p^2\,{}^2P_{3/2,1/2}$ Ba^+ states may be proposed, respectively, according to a Hartree-Fock (HF) calculation.[7] However, by analogy with the $3p$ satellite spectrum of the calcium atom,[34] and taking into account the constant value of the branching ratio, the $5p^5 6s 7s\,{}^2P_{1/2,3/2}$ states of Ba^+, corresponding to the monopole shake up excitation, seem to be more probable.

The shake-down satellites lie too close in energy to the main lines to allow a reliable measurement of their intensities from the photoelectron spectrum. Their intensity, relative to the C main line, was measured from the Auger spectra and is given in Table IV.

The absolute photoionization cross sections for leaving the $Ba^+(5p^{-1})$ ion in an excited state [($G+H$), I, and J] are given in Fig. 9. All of them show the same photon energy dependence, with an enhancement at the opening of the $4d \rightarrow \epsilon f$ channels.

Summing over the intensities of the main and satellite lines allows us to determine the total $5p$ partial photoionization cross section. Its variation over the whole photon energy range is shown in Fig. 10. Our measurements are

TABLE III. Kinetic energies of the Auger electron lines resulting from the decay of a $5p$ hole.

Line	Kinetic energy[a] (eV) This work	Ref. 43[b]	Ref. 44[c]	Ref. 7[d]
1	5.84(2)	5.84	5.85	5.804 (j)
				5.827 (i)
2	5.94(2)	5.91	5.93	
3	6.11(2)	6.09	6.10	
4	6.32(2)	6.29	6.31	
5(A)	6.47(3)	6.43	6.43	6.427 (h)
6	6.74(5)	6.75	6.76	6.773 (g)
			6.81	
7	6.93(4)	6.94	6.95	
				7.001 (f)
8(B)	7.08(5)	7.06	7.06	
9	7.37(5)	7.30	7.29	
10(C)	7.50(2)	7.47	7.48	7.473 (e)
11	7.63(5)	7.57	7.58	7.579 (d)
12	7.98(6)	7.91		
13(D)	8.30(4)	8.30	8.31	8.301 (c)
14	8.40(4)	8.41	8.41	
15	8.62(6)	8.63	8.65	
16	8.84(6)	8.83	8.82	
17(E)	8.97(6)	8.97		
18	9.14(6)	9.09	9.10	
		9.16		
19	9.27(6)	9.28	9.29	
20(F)	9.55	9.54	9.55	9.540 (a,b)
21	9.93(6)	9.86	9.88	
		9.97	9.99	
22	10.17(6)	10.16		
23	10.41(6)	10.41	10.42	
24 } (G)	10.69(6)	10.66	10.63	
25 }	11.47(6)	11.53		
26(H)	11.81(6)	11.81		
27(I)	14.01(6)	14.00	13.96	
28(J)	16.01(6)	16.09	16.14	

[a]The number in parentheses gives the uncertainty on the last figure.
[b]Uncertainty ±0.02 eV.
[c]Uncertainty ±0.09 eV.
[d]The letter in parentheses corresponds to the name given by the authors to the limits of autoionizing series.

TABLE IV. Relative intensities of the shake-down satellites measured at various photon energies from the Auger spectra.

$h\nu$ (eV)	Relative intensity[a] A	B	C	D	E	F
22.9	0.11	0.24	1			
25.3	0.09	0.24	1	0.24		1.00
25.9	0.08	0.22	1	0.22		1.27
43.0[b]	0.15	0.31	1	0.22	0.13	0.98

[a]Relative uncertainty of about 25%.
[b]From the photoelectron spectrum.

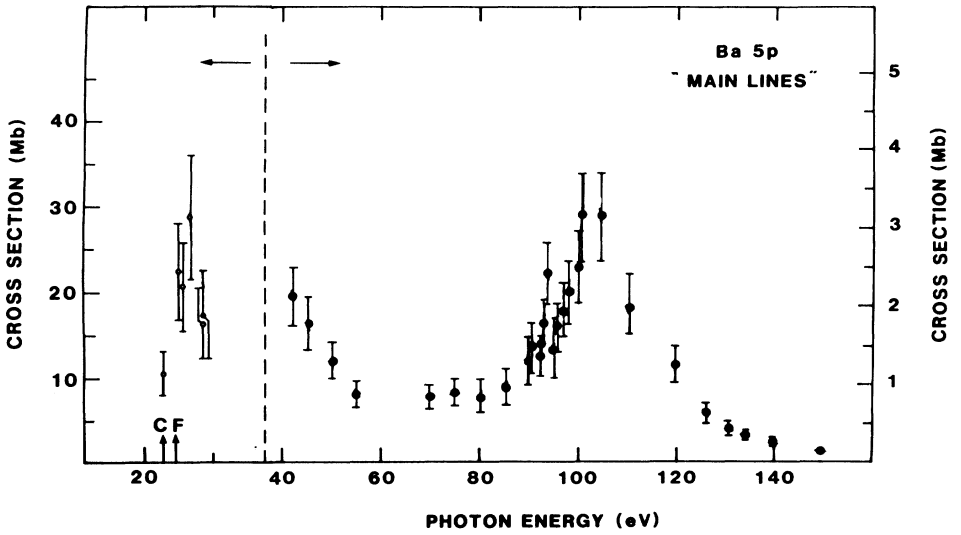

FIG. 6. Variation of the $5p$ photoionization cross section for production of the lines $A-F$ in atomic barium. The measurements are obtained from the intensity of the photoelectron lines ( ) or of the Auger lines ( ).

compared with other values previously obtained in the solid phase[32] and in the vapor.[31] (For the normalization procedure shown in Fig. 2, we had selected some of these points.) For a better comparison, these two other sets of measurements are here normalized to the LDRPA calculated $5p$ cross section,[5] in the same way as ours. The result of this calculation is given in the figure by the continuous line. The agreement with these other measurements is satisfactory. Because of the intrinsic normalization we have chosen, it is meaningless to compare our values with the calculated ones. In fact, there exist a

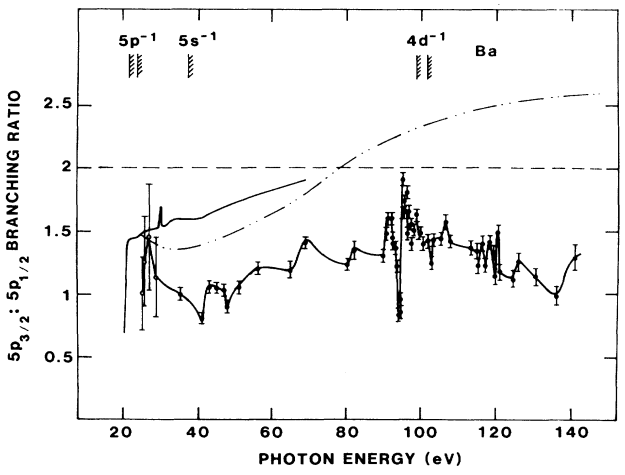

FIG. 7. Variation of the branching ratio $(5p^5 6s^2 J=3/2 : 5p^5 6s^2 J=1/2)$ Ba^+. Present work: measurement obtained ( ) from the photoelectron lines and ( ) from the Auger lines. The theoretical curves are the results of one-electron, Ref. 37 (— ·· —) and LDRPA, Ref. 5 (——) calculations.

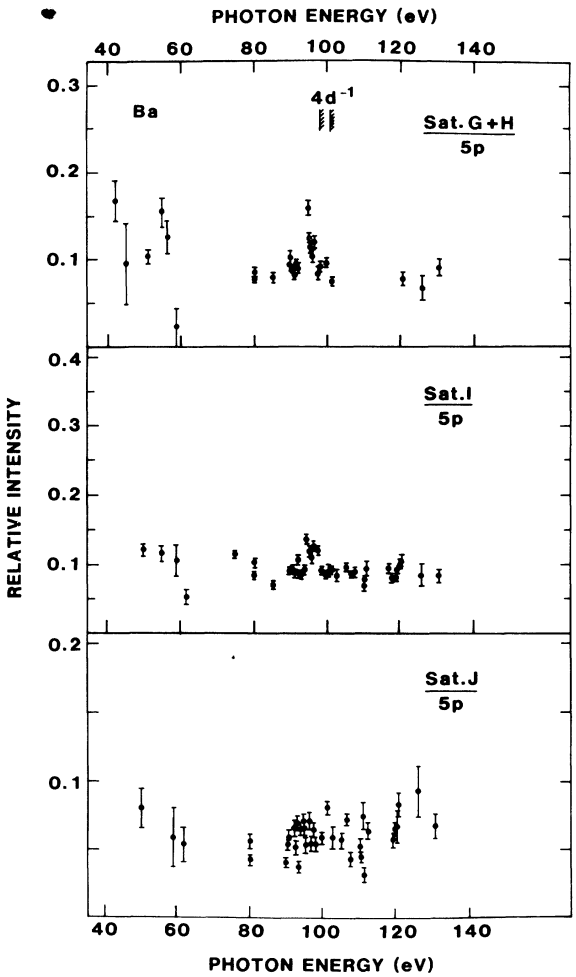

FIG. 8. Variation of the branching ratio between the satellites $(G+H)$, I, J and the $5p$ main lines (lines $A-F$) in barium.

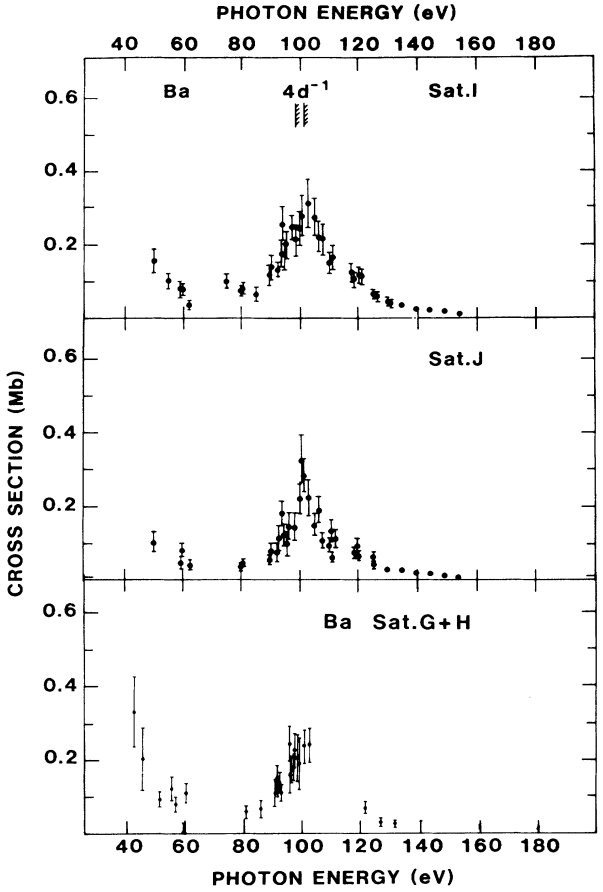

FIG. 9. Variation of partial photoionization cross section in 5*p* subshell of atomic barium with the ion left in various excited states (see Table II).

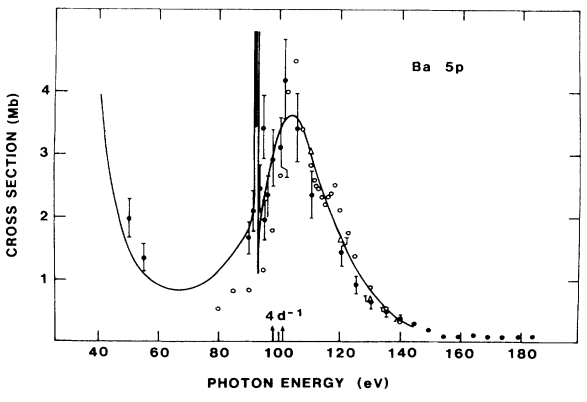

FIG. 10. Variation of the total photoionization cross section in the 5*p* subshell of atomic barium. ⧫, present work; the other measurements are in solid Ba, Ref. 32 (○), and in the vapor (△), Ref. 31. The theoretical curve is the result of the LDRPA calculation, Ref. 5 (——).

wide number of different calculations. It has been shown that, to correctly describe the 5*p* cross section, it is important to include relaxation effects together with interchannel coupling.[12] This is verified for random-phase-approximation (RPA) calculations including relaxation effects,[12] but also for LDRPA (Ref. 5) and time-dependant local density approximation (TDLDA) (Ref. 20) calculations. These two last calculations directly take into account the interchannel interaction, but also use a local density approximation (LDA) potential which simulates a relaxed potential.[46] These three approximations give very close results.

C. Photoionization in 5*s* subshell

Photoionization processes in the 5*s* subshell of a Ba atom may be summarized following the simplified scheme:

$$5s^2\,5p^6\,6s^2\,{}^1S_0\ \mathrm{Ba} + h\nu \xrightarrow{a} 5s\,5p^6\,6s^2\,{}^2S_{1/2}\ \mathrm{Ba}^+ + e^- \Big|_{c} \rightarrow 5s^2\,5p^6\,{}^1S_0\ \mathrm{Ba}^{2+} + e^- \quad (7)$$
$$\qquad\qquad\qquad\qquad \xrightarrow{b} 5s\,5p^6\,nl\,n'l'\ \mathrm{Ba}^+ + e^- \Big|_{c} \rightarrow 5s^2\,5p^5\,(6sx5d)\ \mathrm{Ba}^{2+} + e^-$$

The × in the $(6x \times 5d)$ term means that this state is not a pure eigenstate, but is a mixing of the $5s^2 5p^5 6s$ and $5s^2 5p^5 5d$ configurations.

1. *Photoelectron spectrum*

A 5*s* photoelectron spectrum, obtained at 88 eV photon energy, is shown in Fig. 11, together with the 5*p* and 6*s* photoelectron lines. The different lines we have observed in the 5*s* photoelectron spectrum [processes (7a) and (7b)] are listed in Table V. This was the first measurement of the 5*s* spectrum in atomic barium.[48] The binding energy of the corresponding Ba^+ states is given in column 1, together with a probable assignment in column 3, which is proposed by analogy with the 5*p* photoelectron spectrum. The relative intensity of the lines (column 2) has been measured at 80 eV photon energy.

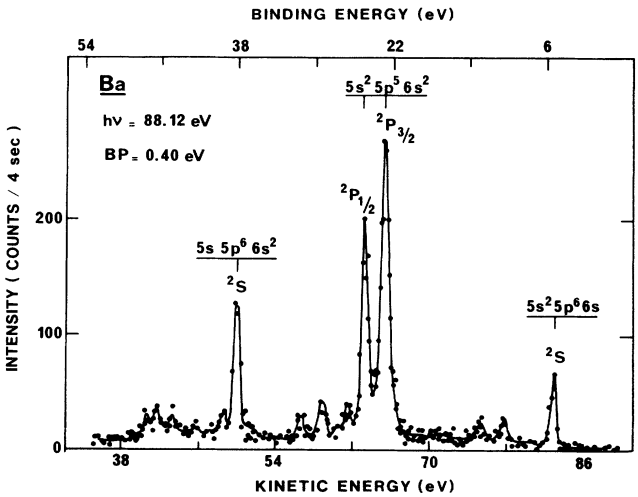

FIG. 11. Electron spectrum recorded at 88 eV photon energy, showing photoionization into the 6*s*, 5*p*, and 5*s* subshells of atomic barium.

TABLE V. Binding energies and possible assignments of the $5s5p^6nln'l'$ Ba^+ ionic states.

Binding energy (eV)[a]	Relative intensity[b]	Possible assignment
38.06(6)	1	$5s5p^6 6s^2\,{}^2S_{1/2}$
39.55(15)	0.20	$5s5p^6(6s^2\times 6s5d\times 5d^2)$
41.85(15)	0.15	
44.60(15)	0.72	$5s5p^6 6s7s$
46.40(20)		

[a]The number in parentheses gives the uncertainty on the last figure.
[b]Measured at 80 eV photon energy.

No shake-down satellite has been observed.

We have not observed any 5*s* Auger line, mainly because of the weak intensity of the 5*s* photoionization process and because the 5*s* hole can decay into many channels [processes (7c)].

2. Cross sections

Our measurements of the 5*s* photoionization cross section between 70 and 150 eV photon energy are reported in Fig. 12. The renormalized measurements in the solid barium[32] show roughly the same agreement with our values as for the 5*p* subshell. The RPA calculations[38] are the closest to our measurements. The agreement with two other many-electron calculations[5,20] is not satisfactory: they are giving results up to a factor 2 higher than our values. The result of a very recent calculation including relaxation and polarization effects[47] does not seem to be in better agreement with our data. However, our points are obtained from the intensity of the lines integrated only between 38 and 42 eV binding energy. Taking a constant contribution of about 60% (measured at 80 eV, see Table V) for the overall intensity of the satellites lines up to around 45 eV binding energy, would raise our measurements in close agreement with TDLDA calculation.

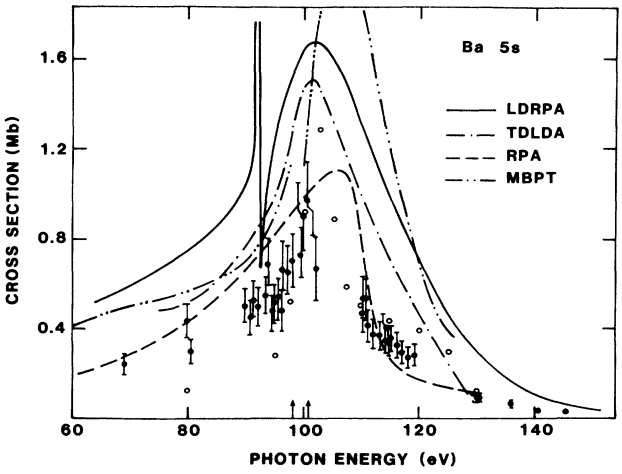

FIG. 12. Variation of the partial photoionization cross section in the 5*s* subshell of atomic barium. ⧫, present work; ○, measurements on solid Ba, Ref. 32. The theoretical curves are the results of RPA, Ref. 38 (— — —); TDLDA, Ref. 20 (—·—·—·); LDRPA, Ref. 5 (——); and MBPT, Ref. 47 (—··—) calculations.

D. Photoionization in 4*d* subshell

A simplified scheme of the 4*d* photoionization processes can be written as

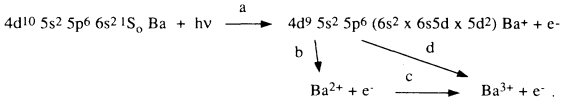

(8)

A general survey of the 4*d* photoelectron [process (8a)] and Auger [process (8b)] electron spectra, obtained at 130 eV photon energy, has been already presented in Fig. 1.

1. Photoelectron spectrum

At the same photon energy of 130 eV, a 4*d* photoelectron spectrum was recorded with twice better resolution. It is given in Fig. 13. The first striking phenomenon is

TABLE VI. Binding energies and possible assignments of the $4d^95s^25p^6nln'l'$ Ba^+ ionic states.

Line	Binding energy[a] (eV) This work	Ref. 11	Ref. 40	Relative intensity[b]	Possible assignment
C'	98.41(6)	98.3(2)	98.5(1)	1	$4d^95s^25p^6 6s^2\,{}^2D_{5/2}$
D'	99.50(10)			0.37	
F'	101.02(6)	101.0(2)	101.0(1)	0.84	$4d^95s^25p^6 6s^2\,{}^2D_{3/2}$
G'	102.20(10)			0.36	
H'	103.10(15)			0.15	
I'	105.25(15)			0.25	$4d^95s^25p^6 6s7s, J=5/2$
J'	107.70(15)			0.15	$4d^95s^25p^6 6s7s, J=3/2$
K'	109.00(15)			0.02	
L'	110.20(15)			0.03	

[a]The number in parentheses gives the uncertainty on the last figure.
[b]Measured at 130 eV photon energy.

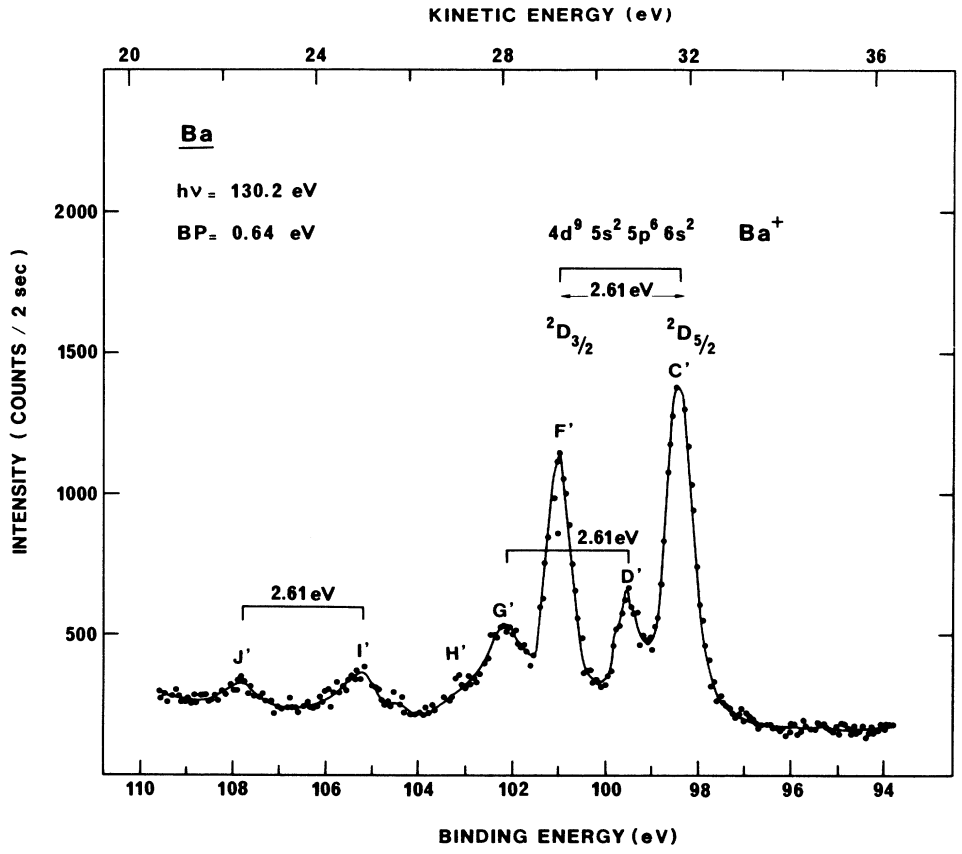

FIG. 13. Photoelectron spectrum resulting from the photoionization in 4*d* subshell, recorded at 130.2 eV photon energy.

the close resemblance with the 5*p* photoelectron spectrum of Fig. 5. The main difference is that we do not observe the existence of shake-down satellites in the 4*d* spectrum, likely because the interaction between the configurations $6s^2$, $6s5d$, and $5d^2$ is weaker in the case of a 4*d* hole than in the case of a 5*p* hole.

To outline the resemblance, we have given the same name (with a prime) to the 5*p* and 4*d* photoelectron lines. The binding energy of the ionic states corresponding to these lines is given in Table VI, column 2. They are compared to previous estimation from the photoabsorption spectrum[11] (column 3) and from the 4*d* Auger spectrum obtained by electron impact[40] (column 4). The relative intensity of the lines (column 5) has been measured at 130 eV photon energy. Finally, an assignment is proposed (column 6) by analogy with the 5*p* spectrum.

It is quite worthwhile to note the strong relative intensity of the 4*d*-satellite channels: the sum of them is equal to about 70% of the 4*d*-main-line channels and contributes to about 40% of the total photoabsorption cross section. Such a high intensity of satellites was already observed a long time ago for xenon,[23,49] although to a lesser extent, since the cross section corresponding to the 4*d* main lines was noted to contribute about 66% to the total cross section, leaving about 33% for the other channels, including the satellite channels.[23] This point has been checked again recently in xenon.[50] Our observations emphasize again that, when comparing theoretical and experimental results, subshell partial cross sections with well-defined initial and final states must be the basis of the comparison and not especially the total cross sections.[22,23]

2. *Auger spectrum*

Nonradiative decay processes of the 4*d* hole are schematized in Fig. 14. The Auger spectrum is basically composed of four structures (see Fig. 1), corresponding to the four main possible final states for the Ba^{2+} ions[40] in process ($8b_i$), where the suffix i ($i=1-4$) is explained in Fig. 14 and in Table VII. The kinetic energy of the main Auger lines which have been observed in these structures (column 2) is given in Table VII. The assignments (column 3) are obtained from the optical data[36,45] for the Ba^{2+} states, from Table VI for the Ba^+ states, and by analogy with the 4*d* Auger spectrum in Xe.[51,52] The structures (b_3) and (b_1) are clearly the most intense ones, reflecting the strong overlap between the wave functions describing a 4*d* hole and a 5*p* electron.

Summing over the whole 4*d* Auger spectrum, we find only a total intensity that is equal to only 40% of the 4*d* photoelectron spectrum intensity. We conclude that, in

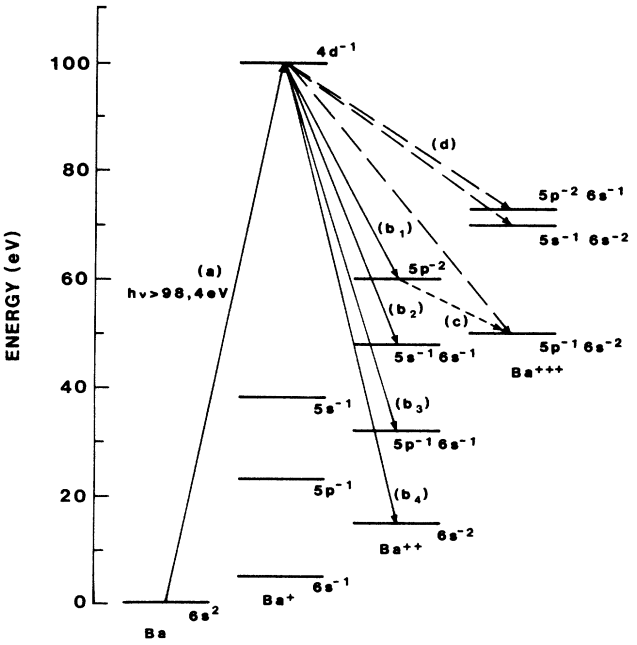

FIG. 14. Simplified diagram of the Ba, Ba^+, Ba^{2+}, and Ba^{3+} levels showing the main decay channels of a $4d$ hole.

60% of the cases, the decay occurs via simultaneous emission of two electrons [process (8d)] or via radiative decay of the $4d$ hole, whose contribution is difficult to estimate. The two electrons share the energy in excess, and contribute to the background in our electron spectra. We have actually observed a sudden and important increase of low-energy electrons when the $4d \rightarrow \epsilon l$ channels are open. Their contribution appears as a continuous distribution between 0 and 30 eV kinetic energy in Fig. 1. A similar phenomenon has been observed in the electron spectrum of Xe at photon energy higher than the $4d$ thresholds.[50] Our assumption is also consistent with a Xe^{3+}:Xe^{2+} ratio of 40% measured at 100 eV photon energy by ion spectroscopy,[53] which confirms the importance of two-electron emission in the Auger decay.

3. *Cross sections*

The variation of the $4d$ photoionization cross section is shown in Fig. 15. Our measurements correspond mostly to the $4d$ main lines, but also include some contribution from the satellite channels that are very difficult to separate from the main lines (up to line H'). Our results are compared with some results previously obtained on the Ba solid[32] and on atomic Ba.[31] For this comparison,

TABLE VII. Kinetic energies and possible assignments of the Auger electron lines resulting from the decay of a $4d$ hole.

Ba^{2+} Final state	Kinetic energy (eV)	Possible assignment[a]
Process (b_1) $5p^{-2}$	34.70	
	36.55	
	37.80	
	39.35	
	40.20	
	41.20	
	42.75	
	43.30	
	45.00	
	45.90	
Process (b_2) $5s^{-1}6s^{-1}$	48.27	$C' \rightarrow 5s5p^6 5d$
	50.20	$C' \rightarrow 5s5p^6 6s$
	51.48	$F' \rightarrow 5s5p^6 5d$
	53.10	$F' \rightarrow 5s5p^6 6s$
Process (b_2) $5p^{-1}6s^{-1}$	60.35	$C' \rightarrow 5p^5 5d\ ^1P_1$
	61.55	$C' \rightarrow 5p^5 6s\ 1/2(1/2)$
	63.40	$C' \rightarrow 5p^5 6s\ 3/2(3/2)_1, 5p^5 5d\ ^3D_1$
		$F' \rightarrow 5p^5 5d\ ^1P_1$
	65.00	$F' \rightarrow 5p^5 6s\ 1/2(1/2)_1$
	66.15	$F' \rightarrow 5p^5 6s\ 3/2(3/2)_1, 5p^5 5d\ ^3D_1$
		$C' \rightarrow 5p^5 5d\ ^3P_1$
	68.40	$F' \rightarrow 5p^5 5d\ ^3P_1$
	69.05	
Process (b_4) $6s^{-2}$	83.30	$C' \rightarrow 5p^6\ ^1S_0$
	85.80	$F' \rightarrow 5p^6\ ^1S_0$

[a] C' and F' denote the ionic configuration of Ba^+ with a $4d$ hole, i.e., $4d^9 5s^2 5p^6 6s^2\ ^2D_{5/2}$ (C') and $^2D_{3/2}$ (F'). (See Table VI.) The Ba^{2+} states are obtained from the optical data (Refs. 35 and 45).

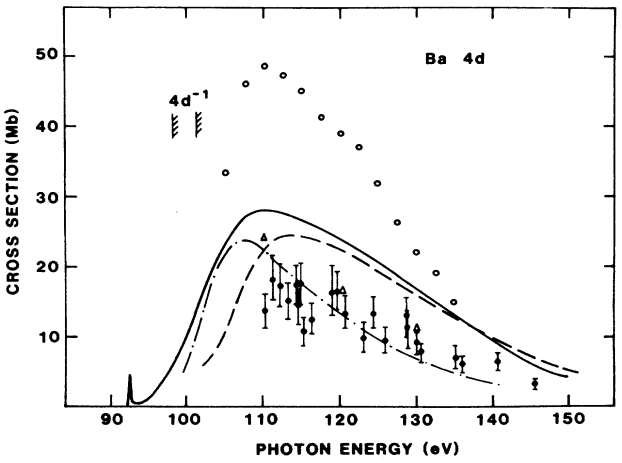

FIG. 15. Variation of the partial photoionization cross section in 4*d* subshell of atomic barium. ⧳, present work. The other experimental results have been obtained in the Ba vapor, Ref. 31 (△) and in solid Ba, Ref. 32 (○). The theoretical curves are the results of a LDRPA calculation, Ref. 5 (——); of a MBPT calculation (—·—·—·, unpublished results of Ref. 47) and of a RRPA-R calculation (— — —, unpublished results of Ref. 54).

these other data have been renormalized in the same way as ours, as explained previously. However, the values on the solid are still twice higher than the ones on the vapor, which underlines again that quantitative information on the atoms must be measured in the vapor phase, especially when the contribution of satellite states is high. The results of our measurements showed[48] lower values of the 4*d* cross section than was generally expected from what was, at this time, the most recent calculations, and from a comparison with photoabsorption data and oscillator sum rule. This was especially true for the height of the maximum. Thus we checked with a special care the transmission of our electron spectrometer as a function of the kinetic energy of the electrons by measuring the ratio between the 5*p* Auger lines and the 5*p* photoelectron lines as a function of photon energy. We found a constant ratio, within our statistical error, which gives us confidence in the validity of our measurements. Also, the few points measured independently in the vapor[31] ar in general agreement with our results. It should be noted, also, that there is no value between 100 and 110 eV photon energy, because the high background of low-energy electrons makes it difficult to determine with accuracy the contribution of the only 4*d* photoelectron lines in this energy region.

In Fig. 15, we have shown the results of three theoretical calculations: LDRPA,[5] many-body perturbation theory[47] (MBPT), and relativistic random-phase approximation with relaxation[54] (RRPA-R). We selected these most recent results from a bunch of at least ten different calculations of the 4*d* cross section. One of the first calculations was performed in the nonrelativistic random-phase approximation with exchange, including only intrashell correlations.[17] In this approximation, the 4*d* cross section peaked at about 80 Mb, which is about four times our present experimental value. With the successive introduction of intershell correlations, relativistic effects, and relaxation effects, the peak value went down, staying however above 40 Mb for a long time.[15,18] A similar behavior was observed in the use of the Hartree-Fock approximation.[19] Further improvement was obtained later when the peak value was lowered to about 30 Mb, as, for example, in the Hartree-Fock relaxed calculations of Kelly *et al.*[19] or in the local-density random-phase approximation of Wendin.[5] Then, very recently, new developments occur in two different approximations. The many-body perturbation theory calculations of Kutzner *et al.*[47] include relaxation and polarization effects, and introduce also a correction to take into account the overlap integrals. The importance of this last parameter seems to be quite high, since the introduction of this effect lowered the overall cross section by about 20%.[47] In the relativistic random-phase approximation with relaxation, the same type of improvement was observed.[54] In Fig. 15, we have plotted as MBPT the average of the relaxed polarized length–relaxed polarized velocity[47] (RPL-RPV) results, which includes both relaxation and polarization diagrams, and the RRPA-R results of Radojevic *et al.*,[54] which include relaxation effects. These two last calculations give the best overall agreement with our experimental results. They are quite similar in magnitude, the shift along the photon energy axis being due to the fact that they did not use the same ionization thresholds in both calculations. A detailed discussion about these new theoretical results can be found in two forthcoming papers.[47,54,55] A more refined description of the two-electron transitions, including double ionization, could further improve the agreement with experiment. It should be pointed out, however, that, for a valuable comparison with the experimental data, any theoretical calculation should make very clear to which final state(s) of the ion correspond a calculated cross section especially whether or not satellite channels are included in the theoretical result.

From the experimental point of view, other progress should be made. The absolute experimental cross sections are determined by normalization to the 5*p* theoretical cross section. Although there is a general agreement on this cross section and the normalization procedure was made over a broad range of photon energies, partial cross sections directly obtained from the only experiment are still needed for a definite comparison with theory. Thus total photoabsorption cross sections measured directly on an absolute scale are highly desired. Also, it should be noted that the double ionization channels, involving the ionization of a 4*d* electron with the ionization of a more outer electron, has been completely ignored in both theory and experiment. Since the intensity of the satellites is so high, one can expect a sizable contribution of the double ionization channels, as was already predicted by the present authors in the case of alkali atoms.[56] With our way of normalization, this would not affect to first order our 4*d* experimental cross section, but the introduction of these channels into the calculations would evidently modify the distribution of the oscillator

strength among all other channels. The fact that some channels are still missing is evident from the integration of our measurements up to 150 eV photon energy: we find an oscillator strength of only 5 and the contribution of the discrete $4d$ excitations will be shown later to be small. The high background of low-energy electrons, which can be observed, for example, in Fig. 1, may be attributed, at least partly, to double ionization channels, since this background shows up only above the opening of the $4d$ channels. The other part is likely coming from multiple Auger decay of the $4d$ hole. Taking into account the entire electron spectrum, including background electrons, in the integration, one obtains a total cross section of about 30 Mb at 115 eV, which would bring the oscillator strength to a value much closer to 10.

IV. RESONANT PHOTOIONIZATION: RESULTS AND DISCUSSION

A. 5p electron excitations

In the $5p$ resonance region, we have the following general scheme for excitation and decay:

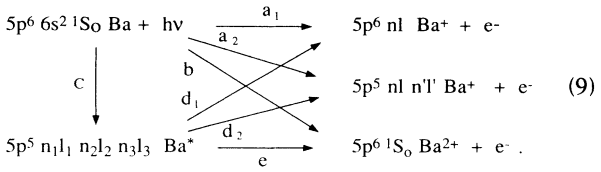

(9)

We have taken photoemission data in this region, between 16 and 22 eV photon energy, with a bandpass of the monochromator equal to 0.11 eV. An electron spectrum obtained in this region, at 21.43 eV photon energy, is shown in Fig. 16. Lines between 5.2 and 15.2 eV binding energy arise mainly from the path [(9c)–($9d_1$)], i.e., resonant ionization in $6s$ subshell via an excited $5p^5 n_1 l_1 n_2 l_2 n_3 l_3$ Ba* atomic state whose excitation energy is included in the bandpass of the monochromator. This explains why the intensity of numerous satellite lines is so high while the direct photoionization [process ($9a_1$)] is of much lower intensity as mentioned previously. Similarly, the few lines at higher binding energy are due to resonant ionization in the $5p$ subshell: while the electrons produced in the process [(9c)–($9d_2$)], i.e., autoionization of a $5p^5 n_1 l_1 n_2 l_2 n_3 l_3$ excited state of neutral Ba to a $5p^5 nln'l'$ excited state of $Ba^+(5p^{-1})$ ion, are at too low a kinetic energy to be detected by our analyzer, we observe here the Auger electron spectrum resulting from the decay of the $5p$ hole in the $Ba^+(5p^{-1})$ ion [process (9f)], leading to doubly ionized Ba^{2+} ion. Some authors used to call this resonant process "two step double ionization."[57,58] Direct photoionization in $5p$ subshell ($9a_2$) contributes also to Ba^{2+} yield via the usual Auger decay (9f).

The $5p$ excitation region has been extensively studied using photoabsorption spectroscopy.[7,8] Most of the resonances have been tentatively classified in more than 14 series converging to 12 thresholds. The assignments we will use for the resonances are taken from these studies.

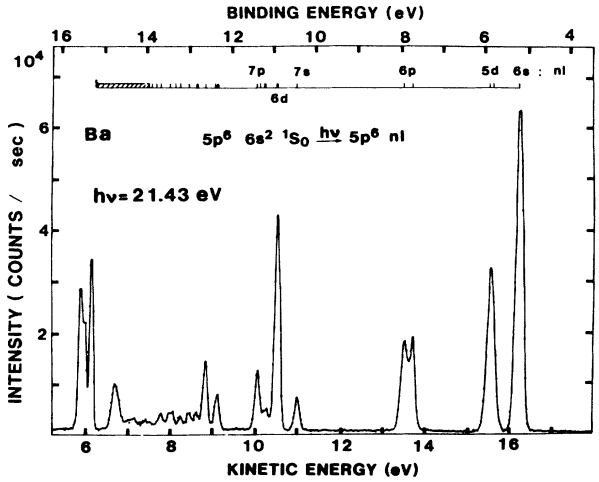

FIG. 16. Electron spectrum recorded at 21.43 eV photon energy in the region of $5p$ electron excitation. The strong enhancement of the $6s$ main line or several $6s$ satellite lines (lines between 6.5 and 16 eV kinetic energy, corresponding to $5p^6 nl$ Ba^+ states), and of some $5p$ Auger electron lines (between 5 and 6.5 eV) results from the autoionization of the $5p^{-1} nl$ Ba* resonant states whose excitation energies are included in the bandpass of the monochromator.

1. Ba^+ decay channels

The excitation functions for the decay channels ($9d_1$) are given in Figs. 17 and 18, for the $nl = 6s$ main line and for the satellite lines up to $nl = 7d$. Absolute values of the cross sections were obtained from the normalization procedure for the $5p$ cross section, as described in the preceding section. The curve for the $5p^6 6p$ channel is shown in both figures for easier comparison. The relative uncertainty in our measurements is estimated to be around 20%, mainly due to the estimation of the density. The absolute uncertainty on the photon energy is 0.03 eV. A second scan between 19.4 and 20.1 eV photon energy, obtained with a better bandpass of 0.07 eV and an uncertainty of 10%, is shown in Fig. 19. It partly overlaps with a previous scan[29] obtained, between 19.7 and 20.8 eV, with a comparable bandpass. The agreement with our results of Figs. 17 and 18 is quite satisfactory, once correction is made for some distortions due to the difference of bandpass, since the value of the cross section at the peak of the resonance is bandpass dependent. The only purpose of the line joining the points in the three figures is to guide the eye.

Looking at these figures, two zones clearly stand out: one between 16 and 19.5 eV photon energy, composed of well-resolved resonances, the other one between 19.5 and 22 eV, exhibiting a high density of resonances. As a specific example, we will comment particularly on the most intense structures emerging from the $6s$ excitation function, and discuss their respective decay modes.

a. Region between 16 and 19.5 eV photon energy. This region is characteized by (i) a small number of channels

available for the decay of the resonances; (ii) an intense line at 17.94 eV, corresponding to the $5p \rightarrow 5d\ ^3P_1$ resonant excitation.

Because of the collapse of the $5d$ orbital in presence of the $5p$ hole, the resonances excited by the external field are of the $5p^5 6s^2 nl$, $5p^5 6s\,5d nl$, and $5p^5 5d^2 nl$ Ba* type, with $l = s$ or d. In this low excitation energy region, only the first members of the series can be populated, mainly $nl = 6s$ and $5d$, to form, in first approximation, $5p^5 6s^2 5d$, $5p^5 6s\,5d^2$, or $5p^5 5d^3$ Ba* states, corresponding to single, double, and triple electron excitations, respectively. Because of the large $5p$-$5d$ wave-function overlap, the way of decay of such resonances is mainly via $5d \rightarrow 5p$ transition, i.e., recombination in the case of $5p \rightarrow 5d$ excitation and Auger decay in the case of $5p \rightarrow 6s$ excitation. Both types of transitions lead to $5p^6 6s$ or $5p^6 5d$ Ba^+ ionic states. This explains why we observe so few decay channels, showing up mainly in the $5p^6 6s$ Ba^+ main electron

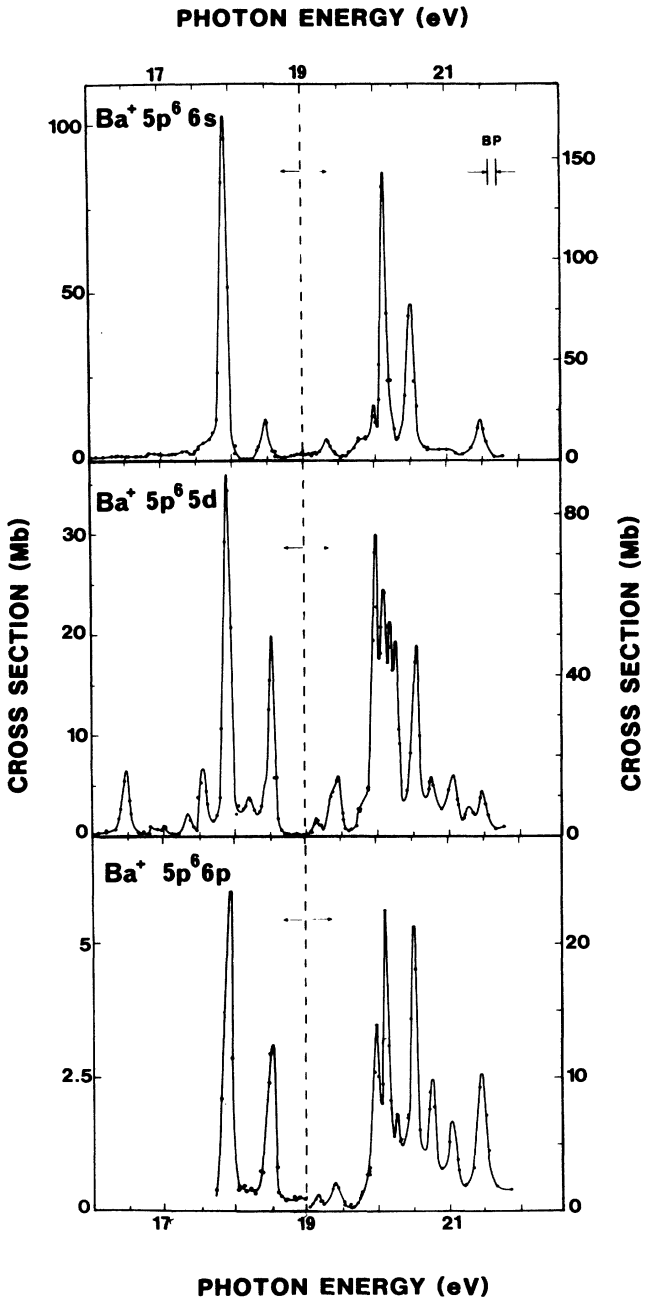

FIG. 17. Excitation functions of the lowest $5p^6 nl$ Ba^+ states ($nl = 6s$, $5d$, and $6p$), obtained between 16 and 22 eV photon energy with a bandpass of 0.11 eV. ●, present work. For this figure and for the following ones, the line between the points only serves to guide the eye.

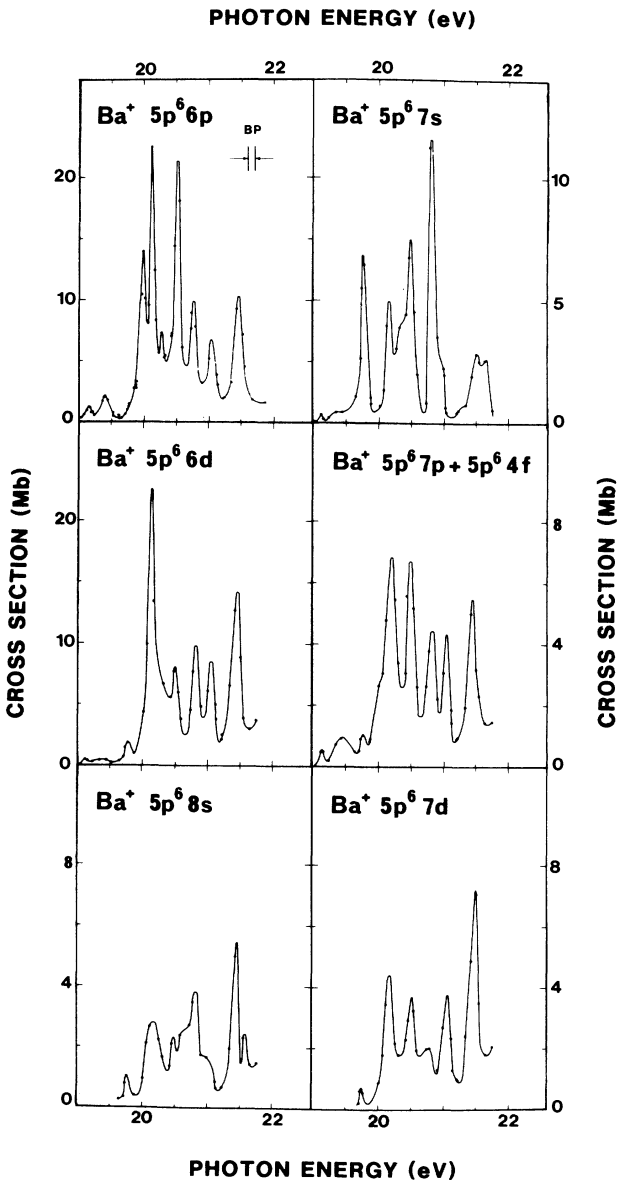

FIG. 18. Excitation functions of the $5p^6 nl$ Ba^+ satellite states, obtained with a bandpass of 0.11 eV.

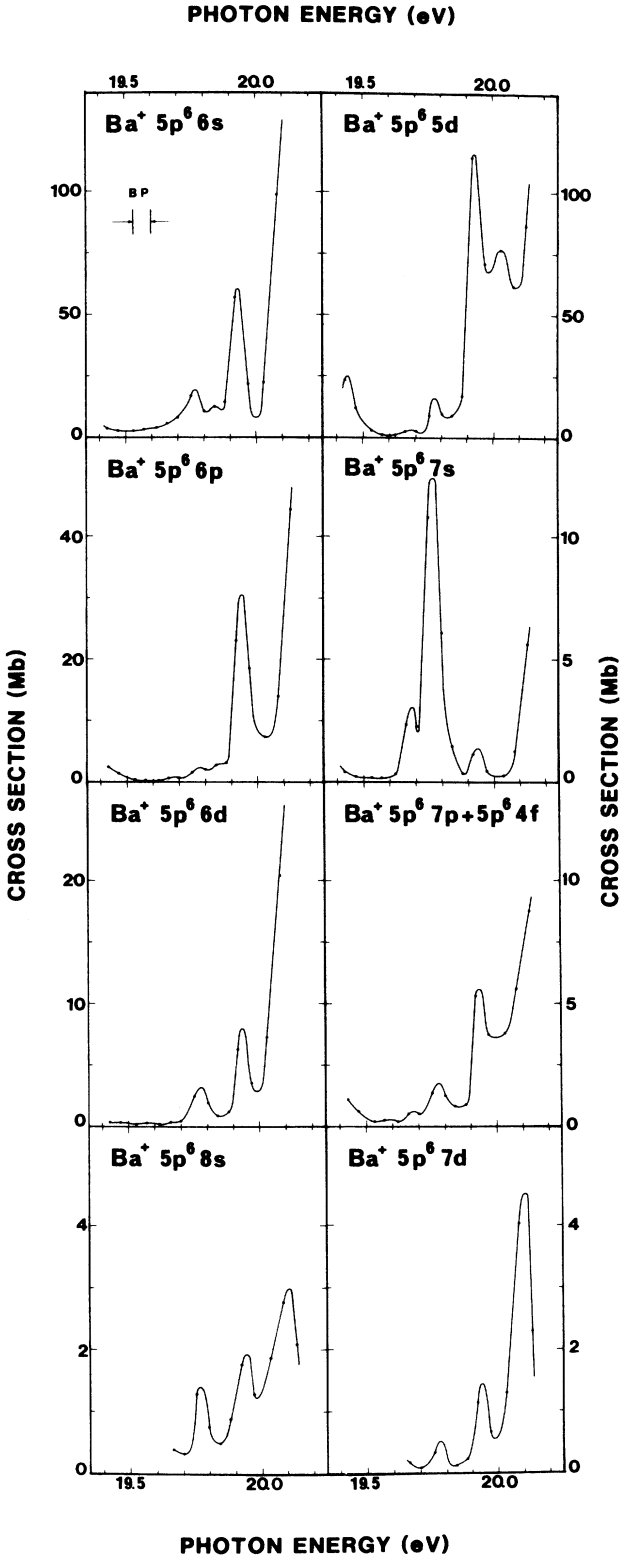

FIG. 19. Excitation functions of the $5p^6nl$ Ba^+ states ($nl = 6s-7d$) obtained between 19.4 and 20.1 eV photon energy with a bandpass of 0.07 eV.

line and in the $5p^65d$ Ba^+ satellite line. Higher satellites have measurable intensity only above 19.5 eV, except for the $5p^66p$ satellite, and we know already from Table III that the ($9d_2$) decay channel to the $5p^5nln'l'$ Ba^+ ionic states will be energetically open only above 21 eV. A more general way of describing the decay scheme would be in terms of configuration interaction, for example, $5p^55d(6s^2+5d^2+6p^2+\cdots)$, allowing the decay to the $5p^66p$ Ba^+ satellite state, in agreement with what we have observed. All these decay processes have been examined in great detail in the similar case of $3p$ electron excitation[33,34] in calcium and we will not discuss them again here.

The case of the $5p \rightarrow 5d\ ^3P_1$ excitation at 17.94 eV is more special. Its similarity with the $3p \rightarrow 3d\ ^1P_1$ giant resonance in Ca is quite striking. First, it exhibits a clear Fano profile in the main $5p^66s$ Ba^+ channel, with a pronounced minimum, close to zero, around 18.2 eV. This minimum does not appear in the other channels, likely because the multiple electron excitation resonances are branching mainly to $5p^6nl$ satellites. These resonances, which lie in the vicinity of the $5p \rightarrow 5d\ ^3P$ intense resonance, derive much of their intensity from interaction with it. A second similarity is its decay mode. The major decay channel is via $5d \rightarrow 5p$ recombination, leading to emission of a $6s$ electron. But we have also observed that the $5p \rightarrow 5d\ ^3P$ resonance is the only one in this energy region branching also to all the nl satellites with intensities detectable in our experiment. We have measured the satellite to main-line branching ratios to be, at the resonance, $5d:6s = 34\%$, $6p:6s = 5\%$, $7s:6s = 0.8\%$, $6d:6s = 0.7\%$, $4f:6s = 2\%$, $7p:6s = 0.4\%$, $8s:6s = 0.7\%$. The branching ratios for the higher satellites are difficult to measure because they mix with $5p$ Auger lines produced by higher-order photons diffracted by the monochromator. Except for the $5d$ satellite, whose high intensity is probably due to the presence of the many-electron excitation resonances, most of these ratios are compatible with those expected, in the off-resonance region, from the ISCI development[39] in Eq. (4). We note in Fig. 17 the existence of such an off-resonance region around 18.8 eV. We measure here the following ratios: $5d:6s = 2\%$, very close to the one predicted by ISCI, and $6p:6s = 5\%$. Thus, in the same way as it was observed for the $3p \rightarrow 3d\ ^1P_1$ giant resonance in Ca, the excitation of the satellites in the case of the $5p \rightarrow 5d\ ^3P_1$ transition in Ba seems to proceed mainly via $5d \rightarrow 5p$ recombination, back to the ground state, followed by emission of an electron into the $5p^6nl$ satellite channels.

When the direct photoionization is weak compared to the resonant photoionization, we are able to measure the oscillator strength for excitation of the isolated resonances. To obtain an absolute value, we have used the signal from direct photoionization in $5p$ subshell by photons diffracted in second order by the monochromator. This signal was recorded simultaneously with the electron spectrum resulting from autoionization of the resonant state. In these conditions, the oscillator strength of the resonance is given by[2]

$$f = 9.69 \times 10^{-3}(I_2/I_1)\Delta h\nu(\Sigma_R/\Sigma_{5p})\sigma_{5p}\ , \qquad (10)$$

where I_2 and I_1 are the photon flux integrated over the bandpass of the monochromator at energy $2h\nu$ and $h\nu$, respectively, $\Delta h\nu$ is the bandpass of the monochromator in first order, Σ_{5p} is the normalized area of the $5p$ photoelectron line, Σ_R is the sum of the normalized areas of the electron lines corresponding to the $5p^6nl$ Ba^+ final states recorded when the monochromator was tuned right at the excitation energy of the resonance, σ_{5p} is the $5p$ photoionization cross section at energy $2h\nu$. $\Delta h\nu$ must be expressed in electron volts and σ_{5p} in megabarns. By this method, we neglect contributions of radiative decay of the resonance and of resonant double ionization, process (9e). Using Eq. (10), we have measured for the symmetrical and isolated resonance at 16.43 eV an oscillator strength $f=0.008\pm0.0015$.

With this value as a reference, we are able to determine the oscillator strength for all the other isolated resonances, from their intensity relative to the resonance at 16.43 eV in the excitation functions. In the case of the $5p\rightarrow5d\ ^3P$ resonance at 17.94 eV, we first verified it is justified to neglect the contribution of direct photoionization, in spite of its Fano profile in the $5p^66s$ Ba^+ channel. From the excitation function, we can estimate the natural width of the resonance, deconvoluting the Voigt profile observed for the resonance from the Gaussian instrumental bandpass. We find then a natural width of 0.02 eV, leading to a value of about 30 for the q-Fano parameter, which confirms the Lorentzian character of the resonance. From the branching ratio of the $5p\rightarrow5d\ ^3P_1$ resonance with the resonance at 16.43 eV, which was obtained by summing over all possible Ba^+ channels, we find $f=0.19\pm0.06$. Using directly Eq. (10), we find $f=0.19\pm0.07$. The excellent agreement between these two measurements confirms the internal consistency of our experimental determinations.

b. Region between 19.5 and 22 eV photon energy. This region is dominated by the $5p\rightarrow5d\ ^1P_1$ giant resonance, around 20.1 eV. Nevertheless, as it was shown in the high-resolution photoabsorption spectra,[8] the large oscillator strength of the resonance is distributed over a wide number of many-electron excitation resonances. The collapse of the $5d$ orbital in presence of the $5p$ hole is once again responsible for this effect, producing a quasidegeneracy of the $5p^56s^2$, $5p^56s5d$, and $5p^55d^2$ configurations. The same process, which was weak in the case of the $5p\rightarrow5d\ ^3P_2$ resonance, is amplified here by a stronger oscillator strength and a higher density of resonances. The decay mode will be the same, i.e., via $5d\rightarrow5p$ recombination, branching mainly to $5p^66s$ Ba^+ main line and to $5p^65d$ Ba^+ satellite, while higher satellite states are being populated via configuration interaction.

In this energy region, we expect to observe also the high members of the $5p\rightarrow ns,nd$ series converging to the various $5p$ ionization thresholds, the lower ones lying around 21 eV. In the case of $5p\rightarrow nd$ transitions, when n is increasing, the $5p^56s^2nd\rightarrow5p^6nd$ Auger-type decay ($5p^{-1}\rightarrow6s^{-2}$ transition), branching to $5p^6nl$ satellites, is constant, while the $5p^56s^2nd\rightarrow5p^66s$ recombination, branching to the $6s$ main line, is decreasing. We expect, therefore, an enhancement of a number of $5p^6nl$ satellites as we go closer and closer to the $5p$ thresholds. In the case of $5p\rightarrow ns$ transitions, the $ns\rightarrow5p$ recombination is always much slower than the Auger-type decay, strengthening the enhancement of the $5p^6nl$ satellites.

Above 21 eV, new decay channels ($9d_2$) are open to $5p^5nln'l'$ Ba^+ continuum states. They correspond to the closest open continua, and contribute to the Ba^{2+} yield by the subsequent Auger decay (9f) of the $5p$ hole. These Ba^{2+} decay channels will be discussed in the next section.

It is not yet possible to use a high enough resolution in such a photoemission experiment to study independently the decay mode of each resonance in this energy region. Thus what was already true in the simplest case of $3p$ excitations in Ca, i.e., that photoemission spectroscopy allows us only in very special cases to isolate a single decay channel for a single resonance, is even truer here. Nevertheless, the moderate resolution we had to use in this work presents the great interest in emphasizing the regions of high oscillator strength density. In that way, the "$5p\rightarrow5d\ ^1P_1$ giant resonance" around 20.1 eV clearly stands out mainly in the $5p^56s$ Ba^+ excitation function, as expected. It appears also distinctly in the $5p^6nd$ Ba^+ satellite channels. Branching to $5p^65d$ Ba^+ results from both $5p^{-1}\rightarrow6s^{-2}$ Auger-type decay and decay of the neighboring double and triple electron excitation resonances taking strength from the giant resonance. Branching to the higher $6d$ and $7d$ satellites seems to arise via a shake-up-type process from the $5d$ satellite state, i.e., $5d\rightarrow nd$ monopole transition occurring during the decay, as is suggested by a constant ($5p^6nd$, $n>5$):($5p^65d$) ratio across the resonance. The same process accounts also for the enhancement, although less pronounced than for the nd satellites, of the $5p^6ns$ ($n=7,8$) Ba^+ satellites. In such a process, the branching ratio ($5p^6ns$):($5p^66s$) must be constant across the resonance. The branching ratio ($5p^6ns$):($5p^66s$) is effectively constant for $n=7$ as can be seen in Fig. 20: there is no enhancement of this ratio at 20.1 eV. We note that the

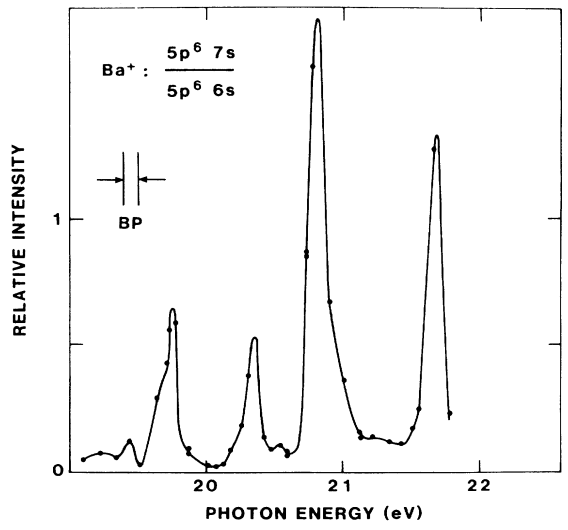

FIG. 20. Variation of the branching ratio ($5p^67s$:$5p^66s$) Ba^+.

same phenomenon occurs for the other intense resonance observed at 20.5 eV in the $7s$ excitation function, which does not show up in the $7s$:$6s$ branching ratio. This conclusion is also true for the weak resonance at 19.84 eV, which is visible in the $6s$ and $7s$ channels only in the high-resolution spectra of Fig. 19.

A second region of high oscillator strength density appears in the $6s$ excitation function around 21.5 eV. It can be attributed mainly to $5p \rightarrow 6d$ transitions, although it is still, in fact, an illustration of $5p^5 6s^2 6d$, $5p^5 6s 5d 6d$, and $5p^5 5d^2 6d$ configuration mixing. Branching to the $5p^6 6d$ Ba^+ satellite is particularly dominant (see also the electron spectrum in Fig. 16, taken in this energy region), which confirms the $6d$ character of this group of resonances, and the increasing importance of $5p^{-1} \rightarrow 6s^{-2}$ Auger decay over the $6d \rightarrow 5p$ recombination. Decay to the $6d$ satellite state is even more intense than for the $5d$ one, as is demonstrated by the $(5p^6 6d)$:$(5p^6 5d)$ branching ratio shown in Fig. 21. At 21.5 eV, the branching ratio exceeds the value of 1 for the first time.

On the high-energy side of the excitation functions, we note a clear decrease of the intensity of the first $5p^6 nl$ Ba^+ states ($nl = 6s - 7s$). On the other hand, the excitation functions of the higher $5p^6 nl$ Ba^+ states gain strength, showing that highly excited $5p \rightarrow nl$ resonances dominate this region, and autoionize mainly via the Auger effect. The increasing behavior of the $(5p^6 6d)$:$(5p^6 5d)$ Ba^+ branching ratio in Fig. 21 is another clear illustration of this process.

2. Ba^{2+} decay channel

The opening of the ways to the Ba^{2+} decay channel occurs just above the first $5p$ ionization threshold, which we have measured to be around 21 eV in the investigation of the shake-down satellites (see Table III). The fast Auger decay (9f) of the $5p$ hole in a $5p^5 nln'l'$ excited state of Ba^+ leaves then a doubly ionized ion in its ground state. We have already explained why we cannot observe here the autoionization process populating this excited state, i.e., the nonradiative transition: $5p^5 n_1 l_1 n_2 l_2 n_3 l_3$ $Ba^* \rightarrow 5p^5 nln'l'$ $Ba^+ + e^-$.

Four Auger spectra, obtained at different photon energies, are shown in Fig. 22. The kinetic energy corresponding to the double ionization threshold is indicated by the vertical hatched line on each spectrum. Strictly speaking, the lines located at kinetic energy higher than this threshold correspond to $5p^6 nl$ Ba^+ ionic states, whereas the ones at lower kinetic energy arise from Auger decay to the Ba^{2+} ion. We note, first, a multiplication of the number of Auger lines as the photon energy increases, because more and more $5p^5 nln'l'$ ionization channels of Ba^+ are open and, second, that the resonant behavior of their intensity is evident.

Having a closer look at the spectra, it appears that the Auger lines seem to emerge as a resonant band of $5p^6 nl$ Ba^+ Rydberg states at photon energy far below their respective $5p^5 nln'l'$ Ba^+ thresholds. This phenomenon, already observed in the vicinity of $3p^5 nln'l'$ Ca^+ thresholds,[33] has been discussed by Wendin elsewhere:[5,59] at a photon energy just below the threshold, a $5p$ electron is resonantly excited and trapped into a quasicontinuum of Rydberg states. Each highly excited Ba state will autoionize preferentially, as we have seen, to the $5p^6 nl$ ($n > 10$) Rydberg satellite state via Auger-type decay. When the photon energy is increased, the resonance crosses the double ionization threshold, and appears as a true Auger line. Just above the threshold, another process takes place to increase the energy of the Auger electron, the classical post-collision interaction (PCI). However, the magnitude of this PCI effect is not expected to be very high, if one takes into account the longer lifetime of the inner hole, as compared to the reference case of the $4d$ hole in xenon.[60,61] The combined effect of these processes is summarized in Table VIII, where is given the

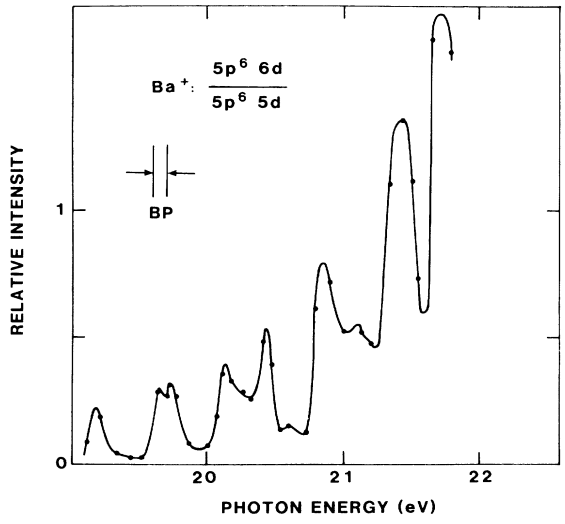

FIG. 21. Variation of the branching ratio $(5p^6 6d$:$5p^6 5d)$ Ba^+.

TABLE VIII. Variation of the kinetic energy of some $5p$ Auger electron lines as the photon energy moves across the lower $5p$ ionization thresholds.

	Kinetic energy of the lines (eV)[a]				
$h\nu$ (eV)	1	2	3	4	5
20.73	6.20				
20.88	6.15				
21.00	5.99				
21.06	5.88				
21.12	5.87		6.23		
21.13	5.87		6.21		
21.21	5.84	5.95	6.09		
21.22	5.86	5.95	6.14		
21.34	5.88	5.95	6.10		6.76
21.43	5.85	5.97	6.11		6.66
21.55	5.86	5.94	6.08	6.33	6.56
21.66	5.84		6.11	6.32	6.48
21.78	5.84		6.11	6.32	6.47

[a]The numbers 1–5 refer to the labeling of the Auger lines as indicated in Fig. 22.

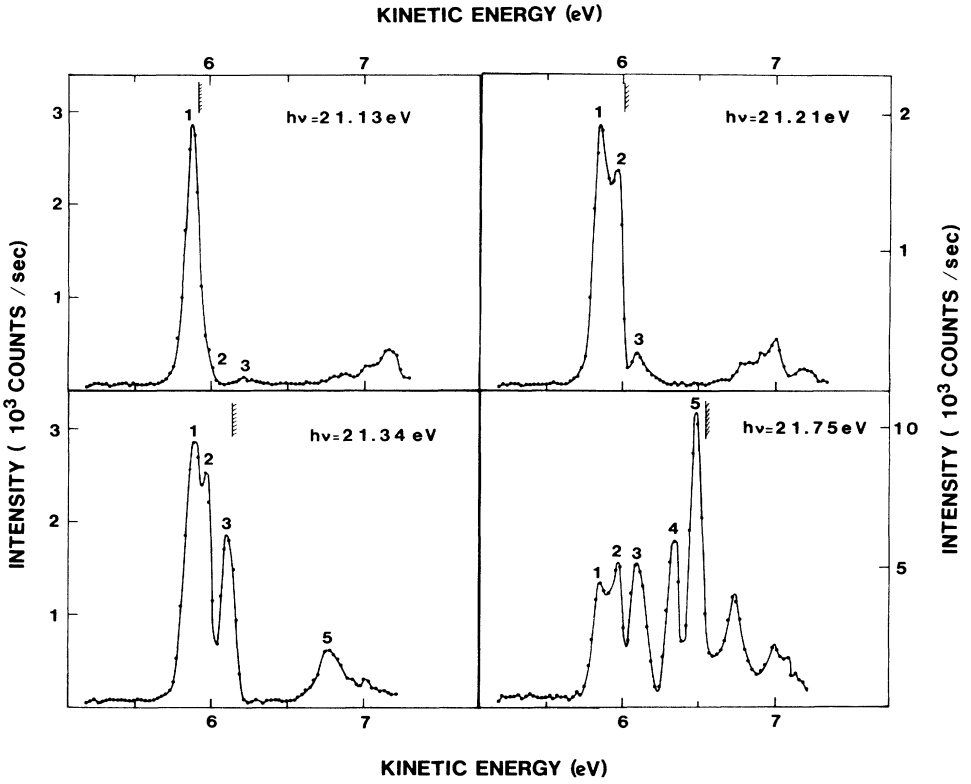

FIG. 22. Four $5p$ Auger spectra recorded at different photon energies between 21.13 and 21.75 eV.

variation, with photon energy, of the kinetic energy of the Auger lines (or pseudo-Auger-lines below the threshold) we have measured.

We observe the first line at 5.84 eV kinetic energy, when it is not affected by PCI. It does correspond to the two Auger lines B and C which have been previously observed in electron spectrometry with the He I emission line,[25] and which are not resolved here. It is interesting to remember that the first observation of these Auger lines by Hotop and Mahr[25] was the key point for the explanation of the anomalously high rate of Ba^{2+} ion measured by Brehm and Höfler[24] with this He I emission line, at 21.22 eV. The energy of these lines is compared to the i and j limits identified in the photoabsorption spectra (see Table III). The interpretation of the photoabsorption spectrum[7] concludes also to the existence of two lower limits k and l. We have not observed any Auger line corresponding to these thresholds; neither have they been observed by electron impact,[43,44] nor have they been detected from any clear enhancement of Ba^{2+} yield appearing at these energies.[62,63]

Following the variation, with photon energy, of the intensity of these Auger lines above the threshold allows us to determine each individual excitation function of the excited Ba^{+} states decaying to the Ba^{2+} exit channel. The sum of them is shown in Fig. 23. The position of the limits $g-k$, extracted from the photoabsorption spectrum, is indicated at the top of the figure. Our points do not include contribution from direct double ionization

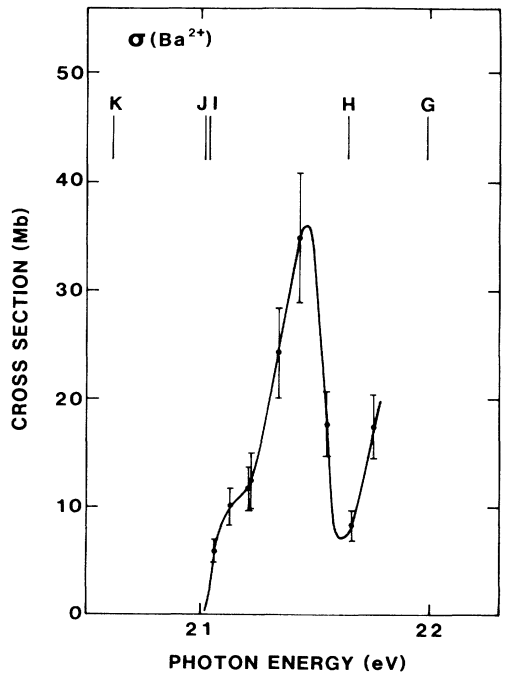

FIG. 23. Excitation function of the Ba^{2+} decay channel. Assuming the radiative decay of the $5p$ hole is negligible, it is equivalent to the excitation function of the $5p^5nln'l'$ Ba^{+} channels.

[process (9b)], or from double autoionization [processes (9c)–(9e)]. The strong fluctuations we observe in the excitation function are associated both with the opening of the new ionization thresholds and with resonant decay to the Ba^{2+} ions [path $(9c+9d_2+9f)$], in particular for the $5p \rightarrow 6d$ resonance at 21.5 eV. It is clear, now, that the apparently special case of excitation with He I emission line, at 21.22 eV, is a particular example of a very general behavior, reflecting the high density of autoionizing states of neutral Ba in this energy region; in fact, the maximum in the intensity of the Auger lines is close to 21.40 eV photon energy with our 0.11 eV monochromator bandpass.

Finally, summing the contributions of all the Ba^+ and Ba^{2+} exit channels, we can obtain the excitation function shown in Fig. 24, which must be roughly equivalent to the photoabsorption spectrum. It is compared to a photoabsorption spectrum[58] taken with a resolution five times better than ours. The absorption spectrum we reconstruct must be slightly underestimated in intensity, because we neglect contributions from direct double ionization, radiative and double ionization decays. Neglecting the first effect should slightly lower the background level in our spectrum, while neglecting the other ones should decrease the intensity of the resonances. However, it is worthwhile to note that, within our normalization, we are able to provide here an absolute scale for the photoabsorption cross section. Because of the difference in the resolution of both experiments, the areas under the main groups of structures should be compared and not the values at the maximum of the resonances. In particular, this explains why we find a much higher cross section at the top of the $5p \rightarrow 5d\ ^1P_1$ resonance, at 20.1 eV, compared to the $5p \rightarrow 5d\ ^3P$ resonance at 17.94 eV. Once this correction has been done, both spectra compare rather well.

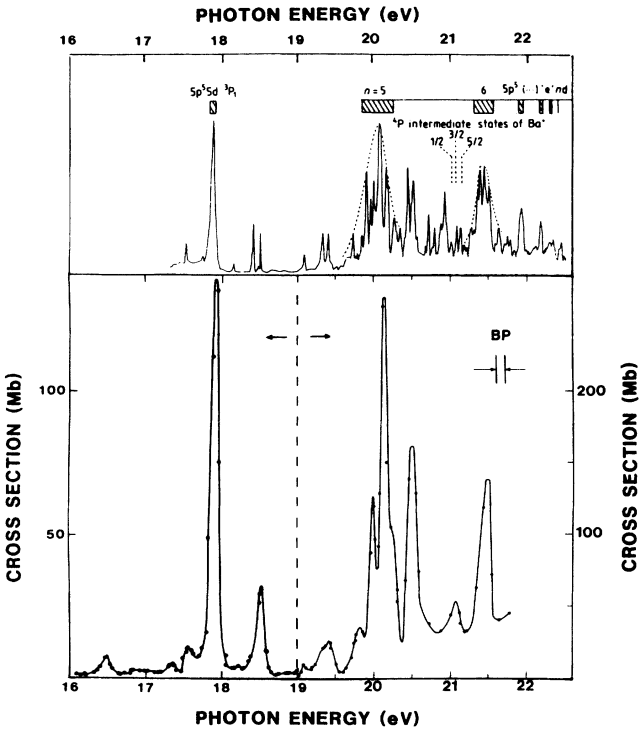

FIG. 24. Excitation function for the sum of the Ba^+ and Ba^{2+} exit channels measured from this photoemission experiment (bottom). In addition to our larger excitation bandpass, the differences with the photoabsorption spectrum (top, from Ref. 58) are due to radiative and resonant multiple ionization decay channels which are not incuded in our measurements.

From the integrated area of this total excitation function, we can estimate a lower limit for the oscillator strength for all the discrete excitations of $5p$ electron up to 22 eV photon energy. Subtracting the relative contribution of the direct photoabsorption in the $6s$ subshell, which we estimated to be 2.5%,[64] we find a value $f = 1.8 \pm 0.4$ by normalization to the oscillator strength measured for the $5p \rightarrow 5d\ ^3P$ resonance. This is about half of the oscillator strength of 4.1 we have found previously for the direct $5p$ photoionization transitions between 23 and 185 eV photon energy. The sum of the discrete and continuum parts of the spectrum leads thus to an oscillator strength very close to 6 for the whole $5p$ subshell. *A posteriori,* this result confirms that the radiative decay of the $5p$ hole has a very low probability.

B. 4*d* electron excitations

Excitation and decay in the region of $4d$ electron excitations may be summarized by the following scheme:

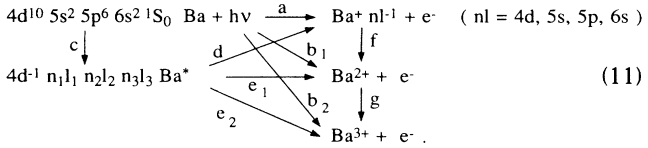

(11)

All the single and multiple ionization thresholds open at these photon energies have already been indicated in Fig. 14. From the early photoabsorption experiments,[9–11] the assignment of the resonances is now rather well established, indicating that the $6s^2$-$6s5d$-$5d^2$ configuration mixing is weak in the case of a $4d$ hole. The $4d$ electron excitation spectrum is composed of some low-intensity resonances below the $4d$ threshold, and of a broad and large maximum in the continuum. The resonances have been identified as discrete $4d \rightarrow 4f\ ^3L$ ($L = P$ near 92 eV, $L = D$ near 96.7 eV) and $4d \rightarrow 6p$ (near 94 eV) excitations.[11] The oscillator strength of the $4d \rightarrow 4f\ ^1P_1$ giant resonance, which might be expected, is in fact shifted into the continuum by the electrostatic interactions, giving rise to the broad maximum[13] shown in Fig. 15. The results for the various photoionization channels in the region of this maximum have been already presented in Sec. III; we will discuss here the decay channels in the region of the discrete excitations.

We show, in Fig. 25, one of the electron spectra we have obtained in this energy region. The photon energy of 94.36 eV corresponds mainly to the excitation energy of the $4d^9 5s^2 5p^6 6s^2 4f\ ^3D$ Ba* resonance.[11] We observe,

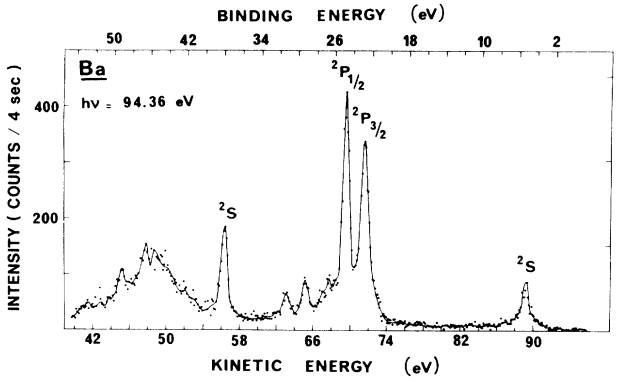

FIG. 25. Electron spectrum recorded at 94.36 eV photon energy, in the region of $4d$ electron excitation, showing from right to left lines arising from ionization in the $6s$, $5p$, and $5s$ subshells. The resonant behavior of the lines is showing up the most clearly, at this energy, in the inversion of the $5p_{1/2}$:$5p_{3/2}$ branching ratio, and in the emergence to the broad and intense structure between 42 and 54 eV binding energy.

in this spectrum, lines arising from photoionization in the $6s$ subshell around 5 eV binding energy, in the $5p$ subshell between 20 and 34 eV binding energy, and in the $5s$ subshell around 38 eV. Compared to the off-resonance spectra (shown in Fig. 11 at 88 eV photon energy), new features attest to the resonant behavior of the lines: the $5p_{3/2}$:$5p_{1/2}$ branching ratio is completely inverted, and a broad structure, composed of numerous unresolved lines, appears between 40 and 54 eV binding energy. We have continuously followed the variation in intensity of these different electron lines between 90 and 102 eV photon energy, with a monochromator bandpass of 0.55 eV. The excitation functions we have measured for the $5p^6(6s,5d)$ (the lines are not resolved at these kinetic energies), $5p^5 6s^2$ (lines $A-H$), $5p^5 nln'l'$ (satellites I and J), $5s5p^6 6s^2$ Ba^+ channels and for the broad structure between 42 and 54 eV binding energy are given in Fig. 26. The excitation function for the $5p$ main lines (in fact, for the $A-H$ unresolved lines) is shown again in Fig. 27, together with the variation of the $5p_{3/2}$:$5p_{1/2}$ branching ratio obtained from the peak value of the lines. From these

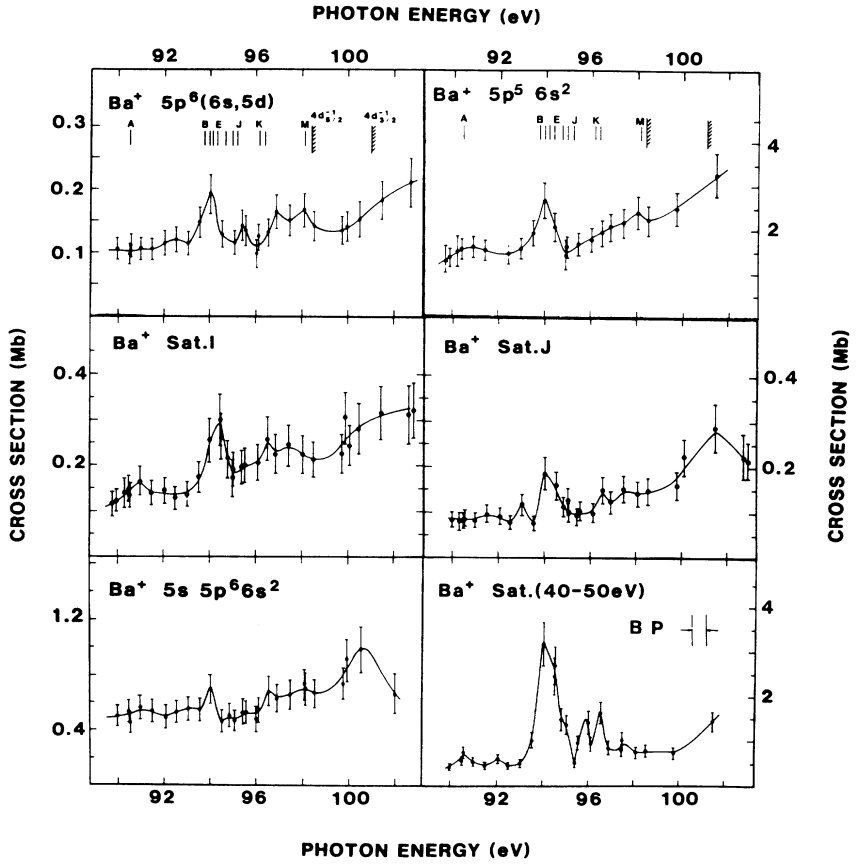

FIG. 26. Excitation functions, between 90 and 102 eV photon energy, of the $5p^6(6s,5d)$, $5p^5 6s^2$, $5p^5 nln'l'$ (satellites I and J), $5s5p^6 6s^2$ states of Ba^+ and of the broad structure between 42 and 54 eV binding energy, corresponding probably to the $5p^4 6s^2 nl$ Ba^+ states.

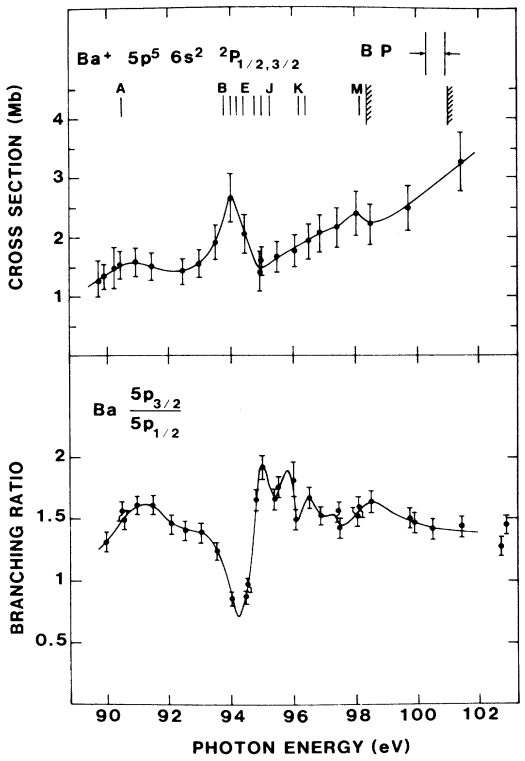

FIG. 27. Top: excitation function of the $5p^5nln'l'$ Ba^+ decay channels (lines $A-H$); bottom: variation, with photon energy, of the branching ratio ($5p^56s^2, J=3/2$:$5p^56s^2, J=1/2$).

results, we can draw some information on the different decay processes

First of all, we note the small intensity in the $5p^66s$ Ba^+ channel. This indicates that the decay of the resonances via $4f \rightarrow 4d$ or $6p \rightarrow 4d$ recombination is weak, as it is expected, because of the small overlap of the $4f$ and $6p$ orbitals with the $4d$ orbital. Auger-type decay is thus dominating, in such a way that we can take advantage of our observations on the $4d$ Auger spectrum to deduce what are the main decay mechanisms of the $4d^9nl$ Ba^+ resonances.

In the case of direct photoionization into the continuum, we have observed that the most intense Auger decay process of the $4d$ hole occurs by simultaneous emission of mainly two electrons. The same is likely true for the decay of the $4d$ resonances [processes (11e)]. The electrons emitted during this process share the excess in energy, and contribute only to the background in our spectra; thus we cannot quantify its contribution. Nevertheless, it should be comparable to what we have previously estimated for the Auger decay of the $4d$ hole, in the order of 60%. This value is of the same order of magnitude as the 75% estimated in the related case of $4d \rightarrow 6p$ excitations in xenon.[50]

From the Auger spectrum (see Fig. 1), we know that the next most intense decay channel occurs when a $5p$ electron fills the $4d$ hole: this is due to the fact that the $5p$ and $4d$ orbitals present the largest overlap. The corresponding decay schemes we have observed are

$$4d^9\,5s^2\,5p^6\,6s^2\,nl\;Ba^* \longrightarrow 4d^{10}\,5s^2\,5p^4\,6s^2\,nl\;Ba^+ + e^- \quad (12a)$$
$$\searrow\; 4d^{10}\,5s^2\,5p^5\,6s\,nl\;Ba^+ + e^- \quad (12b)$$
$$\searrow\; 4d^{10}\,5s^2\,5p^5\,6s^2\;Ba^+ + e^- . \quad (12c)$$

To simplify, we have omitted in this scheme the $6s^2$-$6s5d$-$5d^2$ configuration interaction in the Ba^+ states. The first process (12a), where a $5p$ electron is emitted, is equivalent to the Auger process ($8b_1$) in Fig. 14, and gives the most intense structure in the Auger spectrum (see Fig. 1). It branches to $5p$ satellites (shakes-up satellites with $nl=6p$), in which a second $5p$ electron has been excited. It corresponds to the broad structure we have observed around 47 eV binding energy in Fig. 25 which can be mainly assigned to $5p^46s^2nl$ Ba^+ states. The excitation function of these satellites, given in Fig. 26, emphasizes the strong resonant enhancement of their intensity at each resonance excitation energy, especially at 94 eV ($4d \rightarrow 6p$ excitation). The $5p \rightarrow 4d$ decay transition may also be accompanied by the emission of an outer electron: a $6s$ electron [process (12b), equivalent to the ($8b_3$) Auger decay] branching to the $5p$ satellites, in which transition the second electron is excited from the outer shell, or the nl electron [process (12c)] leading to the $5p$ main lines and satellite lines $A-H$. The excitation function for these lines, given in Fig. 27, shows a strong intensity, which is enhanced at a few resonances. These resonances are more apparent in the $5p_{3/2}$:$5p_{1/2}$ branching ratio.

The other Auger decays of the $4d$ hole are much less intense. A $5s$ electron can fill the $4d$ hole [path ($8b_2$) in Fig. 14)], according to

$$4d^9\,5s^2\,5p^6\,6s^2\,nl\;Ba^* \longrightarrow 4d^{10}\,5s\,5p^6\,6s\,nl\;Ba^+ + e^- \quad (13a)$$
$$\searrow\; 4d^{10}\,5s\,5p^6\,6s^2\;Ba^+ + e^- . \quad (13b)$$

Process (13a) branches to $5s$ satellites, contributing also to the structure between 42 and 54 eV binding energy; process (13b) branches mainly to the $5s$ main line, whose excitation function exhibits a less pronounced influence of the resonances.

Finally, the outer electrons can fill the $4d$ hole, [path ($8b_4$) in Fig. 14]:

$$4d^9\,5s^2\,5p^6\,6s^2\,nl\;Ba^* \longrightarrow 4d^{10}\,5s^2\,5p^6\,6s\;Ba^+ + e^- \quad (14a)$$
$$\searrow\; 4d^{10}\,5s^2\,5p^6\,nl\;Ba^+ + e^- . \quad (14b)$$

Either the nl electron is ejected, leaving an ion in its ground state, or the second $6s$ electron is emitted, branching to $6s$ satellites. The excitation functions for the main $6s$ and $5d$ satellite lines, shown in Fig. 26, have indeed weak intensity, but show clear enhancement at almost each resonance energy.

Finally, as in the case of the $5p$ excitation region, we have summed all Ba^+ exit channels and we compare this result with the measured photoabsorption spectrum[11] in Fig. 28. Above the $4d$ thresholds, the increasing of the cross section is less important in our spectrum, because we have not included the contribution from the dominat-

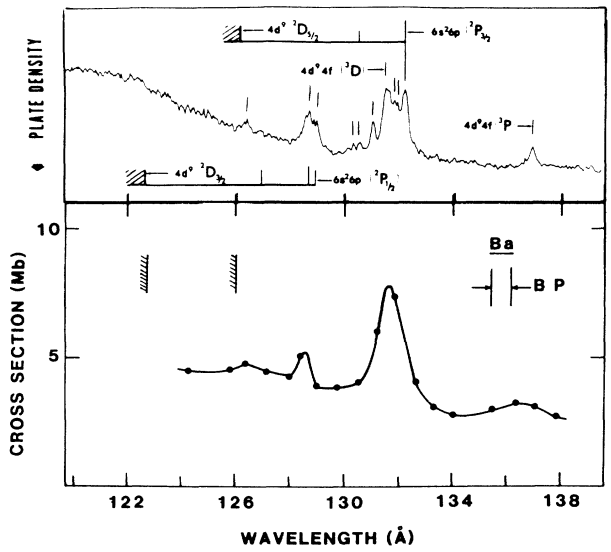

FIG. 28. Comparison between the excitation function of the sum of the Ba^+ channels (bottom) measured in the present work, and the photoabsorption spectrum (top, from Ref. 11).

ing $4d \rightarrow \epsilon l$ channels. Out of this, we find the same structures with a comparable relative intensity taking account of our lower resolution. This seems to indicate that there is no $4d^{-1}nl$ Ba^+ resonance decaying only to a channel we cannot measure, like resonant multiple ionization or radiative decay.

V. SUMMARY AND CONCLUSIONS

Photoionization of $6s$, $5p$, $5s$, and $4d$ subshells of atomic barium has been studied experimentally by electron spectrometry, using synchrotron radiation in the 16–180 eV photon energy range. The excitation energy of a number of atomic states has been measured, in some cases for the first time, such as the binding energy of the $5s$ electron. A particular attention was paid to the various excited states into which the positive ion can be left by photoionization. The probability of leaving the ion into these correlation satellite states has been measured to be very high, following the creation of a hole in either $5p$ or $4d$ inner subshell. This confirms the importance of introducing correlations to higher orders for describing the ionization processes in atomic barium and suggests that double ionization must have a sizable probability.

Partial cross sections were measured and placed on an absolute scale by normalizing them to the calculated LDRPA $5p$ photoionization cross section. In particular, the $4d$ photoionization cross section has been shown to be lower than predicted by all theories, but two new, yet unpublished, calculations.

We have studied, with a special care, the energy regions around the $5p$ and $4d$ thresholds where resonant excitation of an inner electron and ionization take place. The decay channels of a number of resonances have been investigated in detail, allowing partial identification of the intermediate excited states. Auger transitions can occur, in competition with autoionization in the decay of these excited states, or after direct ionization of an inner electron into the continuum. The $5p$ and $4d$ Auger electron spectra have been measured and analyzed in detail.

The experimental results presented here demonstrate the need for improving the introduction of multiple excitations into the theoretical treatment of photoionization. They emphasize also the requirement for urgent determination of absolute total photoabsorption cross sections in metal vapors in order to allow a more critical test of the theory.

ACKNOWLEDGMENTS

We would like to thank H. P. Kelly, V. Radojevic, and M. Kuntzner for communication of their theoretical results prior to publication and for helpful discussions. Thanks are also due to M. Berland for his help in preparing this manuscript and to the technical staff of the Laboratoire pour l'Utilisation du Rayonnement Electromagnétique (LURE) for their service and cooperation. LURE is a national laboratory jointly sponsored by the Centre National de la Recherche Scientifique, the Commissariat à l'Energie Atomique, and the Ministère de l'Education Nationale.

[1]J. M. Bizau, F. J. Wuilleumier, P. Dhez, D. Ederer, J. L. Picqué, J. L. Le Gouët, and P. Koch, in *Laser Techniques for Extreme Ultraviolet Spectroscopy, Subseries on Optical Science and Engineering Number 2,* Proceedings of the Topical Meeting on Laser Techniques for Extreme Ultraviolet Spectroscopy, AIP Conf. Proc. No. 90, edited by T. J. McIlrath and R. R. Freeman (AIP, New York, 1982), p. 331.

[2]F. J. Wuilleumier, J. Phys. (Paris) Colloq. **43**, C2-347 (1982).

[3]J. M. Bizau, F. J. Wuilleumier, D. L. Ederer, J. C. Keller, J. L. LeGouët, J. L. Picqué, B. Carré, and P. M. Koch, Phys. Rev. Lett. **55**, 1281 (1985).

[4]J. M. Bizau, D. Cubaynes, P. Gérard, and F. J. Wuilleumier (unpublished).

[5]G. Wendin, in *New Trends in Atomic Physics,* 1982 Les Houches Lectures, Session XXXVII, edited by G. Grynberg and R. Stora (Elsevier, New York, 1984), p. 557.

[6]G. Wendin, in *Giant Resonances in Atoms, Molecules and Solids,* edited by J. P. Connerade, J. M. Esteva, and R. C. Karnatak (Plenum, New York, 1987), p. 171.

[7]J. P. Connerade, M. W. D. Mansfied, G. H. Newson, D. H. Tracy, M. A. Baig, and K. Thimm, Philos. Trans. R. Soc. London **290**, 327 (1979).

[8]M. A. Baig, J. P. Connerade, C. Mayhew, and K. Sommer, J. Phys. B **17**, 371 (1984).

[9]J. P. Connerade and M. W. D. Mansfield, Proc. R. Soc. London, Ser. A **341**, 267 (1974).

[10]P. Rabe, K. Radler, and H. W. Wolff, in *Proceedings of the IVth International Conference on Vacuum Ultraviolet Radiation Physics, Hamburg, 1974,* edited by ed. E. Koch, R. Haensel, and C. Kunz (Vieweg-Pergamon, Braunschweig, 1974), p. 247.

[11]D. L. Ederer, T. B. Lucatorto, E. B. Salomon, R. P. Madden,

and J. Sugar, J. Phys. B **8**, L21 (1975).
[12]G. Wendin, in Ref. 10, p. 225.
[13]G. Wendin, J. Phys. B **9**, L297 (1976).
[14]K. Nuroh, E. Zaremba, and M. J. Stott, in Ref. 6, p. 115.
[15]G. Wendin, Phys. Lett. **51A**, 291 (1975).
[16]A. W. Fliflet, R. L. Chase, and H. P. Kelly, J. Phys. B **7**, L443 (1974).
[17]M. Ya. Amusia, in Ref. 10, p. 205.
[18]M. Ya. Amusia, V. K. Ivanov, and L. Chernysheva, Phys. Lett. **59A**, 191 (1976).
[19]H. P. Kelly, S. L. Carter, and B. E. Norum, Phys. Rev. A **25**, 2052 (1982).
[20]A. Zangwill and P. Soven, Phys. Rev. Lett. **45**, 204 (1980); Phys. Rev. A **21**, 1561 (1980).
[21]K. Nuroh, M. J. Stott, and E. Zaremba, Phys. Rev. Lett **49**, 862 (1982).
[22]F. J. Wuilleumier and M. O. Krause, Phys. Rev. A **10**, 242 (1974).
[23]F. J. Wuilleumier, At. Phys. **7**, 493 (1981).
[24]B. Brehm and K. Höfler, Int. J. Mass Spectrom. Ion Phys. **17**, 371 (1975).
[25]M. Hotop and D. Mahr, J. Phys. B **8**, L301 (1975).
[26]S. Süzer, S. T. Lee, and D. A. Shirley, Phys. Rev. A **13**, 1842 (1976).
[27]S. T. Lee, S. Süzer, E. Matthias, R. A. Rosenberg, and D. A. Shirley, J. Chem. Phys. **66**, 2496 (1977).
[28]R. A. Rosenberg, M. G. White, G. Thornton, and D. A. Shirley, Phys. Rev. Lett. **43**, 1384 (1979).
[29]P. H. Kobrin, R. A. Rosenberg, U. Becker, S. Southworth, C. M. Truesdale, D. W. Lindle, G. Thornton, M. G. White, E. D. Poliakoff, and D. A. Shirley, J. Phys. B **16**, 4339 (1983).
[30]D. Handschuh, M. Meyer, M. Pahler, T. Prescher, M. Richter, B. Sonntag, and H. E. Wetzel, J. Phys. (Paris) Colloq. **48**, C9-539 (1987).
[31]U. Becker, R. Hölzel, H. G. Kerkhoff, B. Langer, D. Szostak, and R. Wehlitz, in *Abstracts of Contributed Papers, Fourteenth International Conference on the Physics of Electronic and Atomic Collisions, Palo Alto, 1985,* edited by M. J. Coggiola, D. L. Huestis, and R. P. Saxon (North-Holland, Amsterdam, 1986), p. 12; U. Becker, in *Giant Resonances in Atoms, Molecules and Solids,* Vol. 151 of *NATO Advanced Study Institute, Series B; Physics,* edited by J. P. Connerade, J. M. Esteva, and R. C. Karnatak (Plenum, New York, 1987), p. 473.
[32]M. H. Hecht and I. Lindau, Phys. Rev. Lett. **47**, 821 (1981).
[33]J. M. Bizau, P. Gérard, F. J. Wuilleumier, and G. Wendin, Phys. Rev. Lett. **53**, 2083 (1984).
[34]J. M. Bizau, P. Gérard, F. J. Wuilleumier, and G. Wendin, Phys. Rev. A **36**, 1220 (1987).
[35]C. E. Moore, *Atomic Energy Levels,* Natl. Bur. Stand. (U.S.) Circ. No. 467 (U.S. GPO, Washington, D.C., 1971), Vol. 1.
[36]C. E. Theodosiou, Phys. Rev. A **33**, 2164 (1986).
[37]D. Salzmann and R. Pratt (private communication).
[38]M. Ya Amusia and N. A. Cherepkov, Case Stud. At. Phys. **5**, 47 (1975).
[39]H. Bergeron and A. Valance, Z. Phys. D **6**, 309 (1987).
[40]W. Mehlhorn, B. Breuckmann, and D. Hausamann, Phys. Scr. **16**, 177 (1977).
[41]R. A. Roig, J. Opt. Soc. Am. **66**, 1400 (1976).
[42]S. J. Rose, I. P. Grant, and J. P. Connerade, Philos. Trans. R. Soc. Lond. **296**, 527 (1980).
[43]D. Rassi and K. J. Ross, J. Phys. B **13**, 4683 (1980).
[44]R. A. Rosenberg, S. T. Lee, and D. A. Shirley, Phys. Rev. A **21**, 132 (1980).
[45]J. Reader and G. L. Epstein, J. Opt. Soc. Am. **65**, 638 (1975).
[46]Z. Crljen and G. Wendin, Phys. Rev. A **35**, 1571 (1987).
[47]M. Kutzner, Z. Altun, and H. P. Kelly (unpublished).
[48]J. M. Bizau, Ph.D. thesis, University Paris–Sud, Orsay, 1987.
[49]J. B. West, P. R. Woodruff, K. Codling, and R. G. Houlgate, J. Phys. B **9**, 407 (1976).
[50]U. Becker, T. Prescher, E. Schmidt, B. Sonntag, and H. E. Wetzel, Phys. Rev. A **33**, 3891 (1986).
[51]L. O. Werme, T. Bergmark, and K. Siegbahn, Phys. Scr. **6**, 141 (1972).
[52]H. Aksela, S. Aksela, G. H. Bancroft, K. H. Tan, and M. Pulkkinen, Phys. Rev. A **33**, 3867 (1986).
[53]Th. M. El Sherbini and M. J. Van der Wiel, Phys. Scr. **62**, 119 (1972).
[54]V. Radojevic, M. Kutzner, and H. P. Kelly, Phys. Rev. A **40**, 727 (1989).
[55]The authors are very grateful to M. Kutzner, V. Radojevic, and H. P. Kelly for communication of their results prior to publication and for helpful discussions.
[56]P. Gérard, D. Cubaynes, J. M. Bizau, F. J. Wuilleumier, and F. Larkins (unpublished).
[57]J. E. Hansen, A. W. Fliflet, and H. P. Kelly, J. Phys. B **8**, L127 (1975).
[58]J. P. Connerade and M. A. P. Martin, J. Phys. B **16**, L577 (1983).
[59]G. Wendin, in *Photoionization of Atoms and Molecules,* edited by B. D. Buckley (Daresbury Laboratory, Daresbury, England, 1978), p. 1.
[60]V. Schmidt, S. Krummacher, F. J. Wuilleumier, and P. Dhez, Phys. Rev. A **24**, 1803 (1981).
[61]V. Schmidt, J. Phys. (Paris) Colloq. **48**, C9-401 (1987).
[62]D. M. P. Holland and K. Codling, J. Phys. B **13**, L293 (1980).
[63]B. Lewandoski, J. Gant, H. Hotop, and M. W. Ruf, J. Phys. B **14**, L803 (1981).
[64]D. Cubaynes, Ph.D. thesis, University Paris–Sud, Orsay, 1987.